

POLITECNICO DI TORINO

Master's Degree in Civil Engineering



Master's Degree Thesis

Fire Resistance of Reinforced Concrete Filled Rectangular Hollow Steel Columns

Supervisors

Prof. Alessandro P. Fantilli

Prof. Matías Hube

Candidate

Fernando Mondaca F .

July 2023

Summary

Composite structural elements are extensively employed in construction due to their efficient use of each material's strength, enabling each of them to work in the most favorable conditions. In the case of steel-concrete composite structures, this means allowing concrete to work mostly in compression while it is steel that carries the tension stresses. More specifically, when talking about columns composed of steel tubes filled with reinforced concrete, these kinds of sections present a wide array of advantages born out of their composite behavior, such as reduced cross sections requirements (and more available space for architectural design), fire resistance provided by concrete (as opposed to steel profile alone), reduced construction time and no need for formwork, controlled and reduced creep and shrinkage, among many others.

However, despite all the advantages provided by these columns, their behavior in case of an accidental fire situation is not easy to simulate and often requires complex software analysis. With this in mind, this study has focused on analyzing and understanding the behavior of reinforced concrete-filled rectangular hollow steel columns when exposed to fire conditions (accidental situation as modeled by ISO834 fire curve and load analysis through accidental combination), and the development of a simplified tool that allows for the estimation of the fire resistance of these. Additionally, the method has also been used in a study project with the purpose of verifying its applicability and usefulness as a simplified predesign tool.

This study is divided into 5 chapters. The first one is the introduction, where the basic information regarding the materials contemplated and composite sections can be observed. Additionally, the objectives of this study can be found in this section.

The second chapter is a study of the state of the art on fire resistance calculation for this type of composite column. This has been achieved by means of a thorough analysis of past and current methods used for this purpose, as well as those provided by the current European standards.

The third chapter delves into the methodology and steps followed in the development of the simplified mechanical analysis tool. The thermal response has been obtained through the use of CDM DOLMEN's module IS.FUOCO, and starting from the heat map obtained, the mechanical response tool has been developed in Python. This consists of a simplified 5-point approach that is able to simulate the flexo-compressive behavior of reinforced concrete-filled rectangular hollow steel columns in this situation. This approach has been developed with two different stress-strain relationships for concrete in order to compare the results and applicability of both. These results and a discussion of them can also be found in this section.

The fourth chapter is comprised of a hypothetical recovery project of part of the Torino Esposizioni Complex, currently in disuse. A comparison is made between a traditional reinforced concrete approach and the composite column approach, with the fire resistance of the composite columns being calculated through the 5-point method developed in this study.

The concluding chapter, designated as the fifth and final section, encompasses the essential outcomes and deductions of this study. It emphasizes the most significant findings and conclusions while also suggesting a potential adaptation of the method for future investigations.

Acknowledgements

En primer lugar, me gustaría agradecer a mi familia, quienes, ya sea desde lejos o cerca, me han estado apoyando y orientando a lo largo de este año y medio lejos de casa. No podría haber experimentado este increíble proceso de crecimiento profesional y personal sin su apoyo incondicional, y es algo por lo que estaré eternamente agradecido.

También les quiero agradecer muchísimo a todos mis amigos, tanto aquellos que me han brindado apoyo a distancia como aquellos que han estado cerca o que he conocido en el camino. Su compañía ha sido fundamental para transformar esta oportunidad educativa en una experiencia de crecimiento personal, y no puedo imaginar estos años sin ustedes.

Infine, desidero ringraziare il Professore Alessandro Fantili, l'ingegnere Filippo Venere e tutti i miei colleghi di Essebi. La sua guida durante questo periodo è stata molto importante per me, sia per completare il mio lavoro di tesi sia per diventare un ingegnere migliore. Grazie mille.

Table of Contents

List of Tables	VIII
List of Figures	IX
1 Introduction	1
1.1 Columns and Main Design Parameters	1
1.2 Objectives	2
1.3 Materials	2
1.3.1 Concrete	2
1.3.2 Steel	7
1.4 Composite Sections	9
2 State of the Art on Fire Resistance Calculation - Composite Columns	14
2.1 Eurocode Approach	15
2.1.1 Tabular Method	15
2.1.2 Simple Calculation Model	16
2.1.3 Advanced Calculation Model	18
2.2 Current Research and Proposed Models	19
2.2.1 "Fire Resistance of Rectangular Steel Columns Filled with Bar-Reinforced Concrete" by T.T. Lie and R.J. Irwin [17] . .	19
2.2.2 "Fire Resistance of Steel Columns Filled with Bar-Reinforced Concrete" by T.T. Lie and V. K. R. Kodur [19]	23
2.2.3 "Enhancing the Fire Performance of Concrete-Filled Steel Columns through System-Level Analysis" by R. S. Fike and V. K. R. Kodur [23]	27
2.2.4 "Fire resistance of restrained composite columns made of concrete filled hollow sections" by João Paulo C. Rodrigues and Luís Laím [26]	30
2.2.5 Other Studies	33

3	Mechanical Analysis Tool	34
3.1	Thermal Response Through CDM Dolmen	34
3.2	Mechanical Response	36
3.2.1	Basics of the Model	36
3.2.2	Stress-Strain Relationships	39
3.2.3	Calculation of 5 Point Approach	49
3.3	Results	59
3.4	Discussion	63
3.4.1	Curve with SS relationship for concrete as displayed in figure 3.9	63
3.4.2	Curve with SS relationship for concrete as displayed in figure 3.12 (modified parabola-rectangle)	64
4	Application - Hypothesis of Recovery at Torino Esposizioni Complex	66
4.1	Traditional Reinforced Concrete Approach	67
4.2	Alternative Composite Column Approach	70
5	Conclusions	77
A	Detail of Utilization Factors for Composite Columns Designed	79
	Bibliography	84

List of Tables

1.1	Common concrete strength classes	3
1.2	Comparative results between columns	13
2.1	Values of f_1 and f_2	26
2.2	Various structural configurations and fire scenarios simulated in the building [23], adapted.	30
2.3	Test plan of [26]	31
3.1	Accuracy of the method used, P40x80t10	63
3.2	Accuracy of the method used, P30x60t5	64
3.3	Accuracy of the method used, P40x80t10	64
3.4	Accuracy of the method used, P30x60t5	65
4.1	Fire resistance class of RC columns in traditional approach, per the tabular method in Eurocode 2, part 1-2 [35]	69
4.2	Fire classification of the structure	76

List of Figures

1.1	Typical stress-strain relationship of concrete [5]	3
1.2	Parabola-rectangle diagram for concrete under compression [3] . . .	4
1.3	Confined concrete behavior [3]	5
1.4	Residual compressive strength of concrete at elevated temperatures [6]	6
1.5	Experimental stress-strain curves after heating for different temperatures [7]	6
1.6	Example of spalling in a RC beam [9]	7
1.7	Typical stress-strain relationship of hot rolled steel in traction [10] .	8
1.8	Idealised and design stress-strain diagrams for reinforcing steel (for tension and compression)[3]	8
1.9	Stress-strain curve for steel S280 at different temperatures [11] . . .	9
1.10	Typical cross-sections of composite columns and notation, [12] . . .	10
1.11	Input parameters and results obtained for a RC column 40x40 with 8 ϕ 26 symmetrical reinforcement	11
1.12	$M_x - M_y$ domain, $N = 0$	12
1.13	$M_x - M_y$ domain of composite section, $N = 0$	13
2.1	Table 4.7 of EC4, part 1-2 [15], tabular method for establishing fire resistance of concrete-filled hollow section columns.	16
2.2	Thermal network in quarter section [17]	20
2.3	Load-Deflection Analysis [17]	21
2.4	Temperature along Center line of Column (203 x 203 x 6.35 mm) .	22
2.5	Temperature along Center line of Column (305 x 305 x 6.35 mm) .	22
2.6	Temperature along Center line of Column (254 x 254 x 6.35 mm) .	22
2.7	Calculated and Measured Axial Deformations of Column (203 x 203 x 6.35 mm)	24
2.8	Calculated and Measured Axial Deformations of Column (254 x 254 x 6.35 mm)	24
2.9	Calculated and Measured Axial Deformations of Column (305 x 305 x 6.35 mm)	24

2.10	Calculated Column Strengths as Function of Time and Calculated Measured Fire Resistance	24
2.11	Comparison of Calculated Fire Resistance with That from Tests . .	27
2.12	Comparison of Fire Resistance for Square HSS Columns with Model Predictions	27
2.13	Time-temperature relationship for various fire scenarios [Kmag] . .	28
2.14	Scheme of the cross-sections of the tested columns [26]	32
3.1	Section and materials defined in IS Fuoco	34
3.2	Heat distribution at 30 minutes	35
3.3	Heat distribution at 60 minutes	35
3.4	Heat distribution at 90 minutes	36
3.5	Heat distribution at 120 minutes	36
3.6	5-Point approach	37
3.7	Temperature expected on concrete and structural steel elements at 120 minutes	38
3.8	Temperature expected on reinforcing bars at 120 minutes	38
3.9	Stress-Strain relationship of concrete at higher temperature, in accordance to Eurocode 2 part 1-2 [35]	40
3.10	Relevant deformation values and resistance ratios for concrete, in accordance to [35]	40
3.11	Stress-strain relationship modeled by SSRELC	43
3.12	Stress-strain relationship modeled by SSRELCPROVA	43
3.13	Stress-Strain relationship for steel at higher temperature, in accordance to [36]	44
3.14	Definition of stress-Strain relationship for steel at higher temperature, in accordance to [36]	45
3.15	Relevant ratios for steel at higher temperatures, in accordance to [36]	45
3.16	Stress-strain relationship coded for steel	48
3.17	Behavior of concrete section	55
3.18	Results for P40x40t10 after 120 minutes	59
3.19	$M_z - N$ interaction domain after 30 minutes, P40x80t10	60
3.20	$M_z - N$ interaction domain after 60 minutes, P40x80t10	60
3.21	$M_z - N$ interaction domain after 90 minutes, P40x80t10	60
3.22	$M_z - N$ interaction domain after 120 minutes, P40x80t10	60
3.23	$M_y - N$ interaction domain after 30 minutes, P40x80t10	60
3.24	$M_y - N$ interaction domain after 60 minutes, P40x80t10	60
3.25	$M_y - N$ interaction domain after 90 minutes, P40x80t10	61
3.26	$M_y - N$ interaction domain after 120 minutes, P40x80t10	61
3.27	$M_z - N$ interaction domain after 30 minutes, P30x60t5	61
3.28	$M_z - N$ interaction domain after 60 minutes, P30x60t5	61

3.29	$M_z - N$ interaction domain after 90 minutes, P30x60t5	62
3.30	$M_z - N$ interaction domain after 120 minutes, P30x60t5	62
3.31	$M_y - N$ interaction domain after 30 minutes, P30x60t5	62
3.32	$M_y - N$ interaction domain after 60 minutes, P30x60t5	62
3.33	$M_y - N$ interaction domain after 90 minutes, P30x60t5	62
3.34	$M_y - N$ interaction domain after 120 minutes, P30x60t5	62
4.1	Torino Esposizioni Complex	66
4.2	Underground floor, reinforced concrete columns	67
4.3	Ground floor, reinforced concrete columns	68
4.4	First-floor, reinforced concrete columns	68
4.5	Roof structural plans	69
4.6	Underground floor, composite columns	70
4.7	Ground floor, composite columns	71
4.8	First-floor, composite columns	71
4.9	Composite columns details	72
4.10	SAP2000 model	72
4.11	Composite columns in SAP2000 model	72
4.12	$M_z - N$ Interaction Domain, P30x60	74
4.13	$M_y - N$ Interaction Domain, P30x60	74
4.14	$M_z - N$ Interaction Domain, P40x80	75
4.15	$M_y - N$ Interaction Domain, P40x80	75
5.1	$M_z - N$ Interaction Domain, P40x40t10, Hybrid Approach	77
A.1	Under ground columns fire classification, P40x80	79
A.2	Ground floor columns fire classification, P40x80	80
A.3	First floor columns fire classification, P40x80	80
A.4	Under ground columns fire classification, P30x60	81
A.5	Ground floor columns fire classification, P30x60	82
A.6	First floor columns fire classification, P30x60	83

Chapter 1

Introduction

1.1 Columns and Main Design Parameters

Columns are the main structural element charged with transmitting the weight of the structure above it over to the structure below it, generally being responsible for the vertical load transfer all the way to the foundations. Considering this, these elements work mostly under compression but also need to be designed for moment and shear in both principal axes to take into account the effect of horizontal loads upon the structure, such as those caused by wind or seismic action.

In general, these are the five internal actions that are the most relevant for designing a column: N (axial load), M_x (bending moment in the x direction), M_y (bending moment in the y direction), V_x (shear in the x direction), V_y (shear in the y direction). Despite all 5 of these internal actions being considered for the design, usually, it is the interaction between the bending moments and the axial load that is the most problematic.

The internal actions considered for design come from the different load combinations provided by the Eurocode [1]. There are several load combinations for both Ultimate Limit State (ULS) and Serviceability Limit State (SLS). In this study in particular, the focus will be on the accidental situation associated with fire (ULS case), which is governed by the load combination observable in equation 1.1.

$$G_1 + G_2 + P + A_d + Q_{k1}\psi_{21} + Q_{k2}\psi_{22} + \dots \quad (1.1)$$

Where G_1 and G_2 correspond to the structural and non-structural self-weight of the structure, respectively, P is the pre-stressing load, A_d refers to the accidental situation under consideration, and Q refers to the variable loads. In the case under study, the A_d component is eliminated from the load combination but a gradual

decrease in the mechanical properties of the structural materials is considered (in association with the duration of the exposure to fire and increment in temperature). Given this situation, the fire verification is conducted for structural elements where a specific qualification is acquired in accordance with the following terminology: RXX, where XX corresponds to the time (in minutes) that the element is designed to resist under fire action.

1.2 Objectives

The objective of this study will be the development of a simplified tool that allows the evaluation of the fire-resistant flexo-compressive properties of a reinforced concrete-filled rectangular or squared hollow steel section column, alongside a review and analysis of the current analytical and empirical methods used for this purpose. This tool will primarily emphasize in the mechanical response of the column, rather than delving into the extensively researched topic of heat distribution within its section. As a result, the commercial software CDM DOLMEN will be employed to derive the heat distribution, and that will be taken as the starting point for the mechanical analysis.

Also, the developed tool will be used in a design project in order to evaluate its applicability and usefulness as a predesign tool, as well as the usefulness of reinforced concrete-filled rectangular hollow steel columns in comparison to traditional reinforced concrete columns.

1.3 Materials

1.3.1 Concrete

Concrete constitutes one of the most widely used substances in the world, only second to water in consumption worldwide [2]. This remarkable fact is related to many factors, among which rank its accessible price, easy and widely studied use, and good mechanical properties.

In general, concrete is classified according to concrete strength classes which relate to its characteristic compressive strength (f_{ck}). This value is determined by the strength of a cylinder test sample after 28 days, but can also be determined on cube samples as $f_{ck,cube}$. The general values found in Europe are the ones shown in table 1.1, in accordance with Eurocode 2, table 3.1 [3].

Strength Classes for Concrete												
f_{ck} (MPa)	12	16	20	25	30	35	40	45	50	55	60	70
$f_{ck,cube}$ (MPa)	15	20	25	30	37	45	50	55	60	67	75	85
f_{ctm} (MPa)	1,6	1,9	2,2	2,6	2,9	3,2	3,5	3,8	4,1	4,2	4,4	4,6

Table 1.1: Common concrete strength classes

However, for safety reasons, the compressive strength used for design is reduced further by two coefficients in order to consider the general inaccuracy associated with concrete mixing in situ as well as the effect of long-term loading on compressive strength. The result can be seen in equation 1.2:

$$f_{cd} = \alpha_{cc} \frac{f_{ck}}{\gamma_c} \quad (1.2)$$

Where the value of α_{cc} varies between 0.8 and 1 depending on the country ($\alpha_{cc} = 0,85$ for Italy), and $\gamma_c = 1,5$ is the partial safety factor for concrete.

As can also be observed in table 1.1, despite having a relatively high compressive strength, concrete lacks the same behavior under tensile stress. The tensile strength of concrete is of only between 8-15% of that of the compressive strength [4], and in most design situations it is considered negligible. This behavior can be clearly observed in figure 1.1.

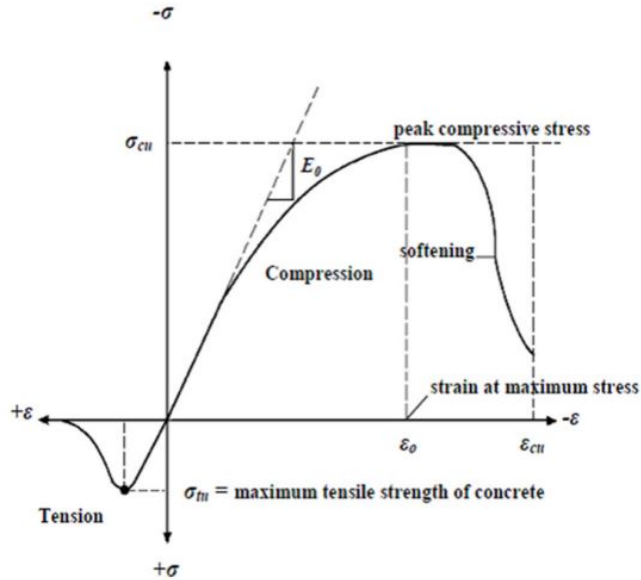


Figure 1.1: Typical stress-strain relationship of concrete [5]

However, the stress-strain relationship portrayed in figure 1.1 is complicated to use for design, reason why the most commonly used stress-strain relationship for this material is the parabola-rectangle diagram under compression. This can be described by equations 1.3 and 1.4, alongside figure 1.2.

$$\sigma_c = f_{cd} \left[1 - \left(1 - \frac{\epsilon_c}{\epsilon_{c2}} \right)^n \right] \text{ for } 0 \leq \epsilon_c \leq \epsilon_{c2} \quad (1.3)$$

$$\sigma_c = f_{cd} \text{ for } \epsilon_{c2} \leq \epsilon_c \leq \epsilon_{cu2} \quad (1.4)$$

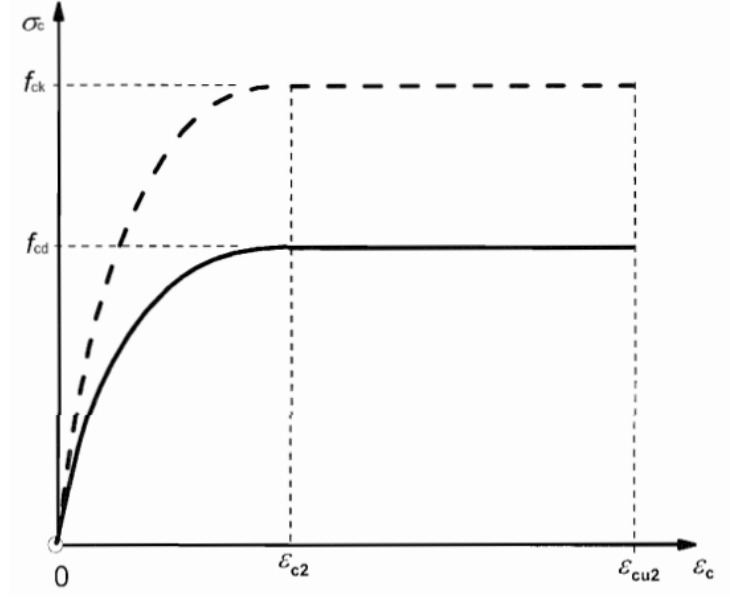


Figure 1.2: Parabola-rectangle diagram for concrete under compression [3]

Another important aspect regarding concrete is the effect of confinement. It has been observed that the compressive strength of concrete increases when this is laterally restrained, and this behavior is currently modeled (in accordance to Eurocode 2, [3]) in the following way:

$$f_{ck,c} = f_{ck} \left[1 + 5 \frac{\sigma_2}{f_{ck}} \right] \text{ for } \sigma_2 \leq 0,05 f_{ck} \quad (1.5)$$

$$f_{ck,c} = f_{ck} \left[1,125 + 2,5 \frac{\sigma_2}{f_{ck}} \right] \text{ for } \sigma_2 \geq 0,05 f_{ck} \quad (1.6)$$

$$\epsilon_{c2,c} = \epsilon_{c2} \left(\frac{f_{ck,c}}{f_{ck}} \right)^2 \quad (1.7)$$

$$\epsilon_{cu2,c} = \epsilon_{cu2} + 0,2 \frac{\sigma_2}{f_{ck}} \quad (1.8)$$

Where $\sigma_2 = \sigma_3$ represents the confinement pressure applied on the concrete element, and the other parameters denoted by the sub-index c refer to those that describe the behavior under confinement. This can also be visualized in figure 1.3.

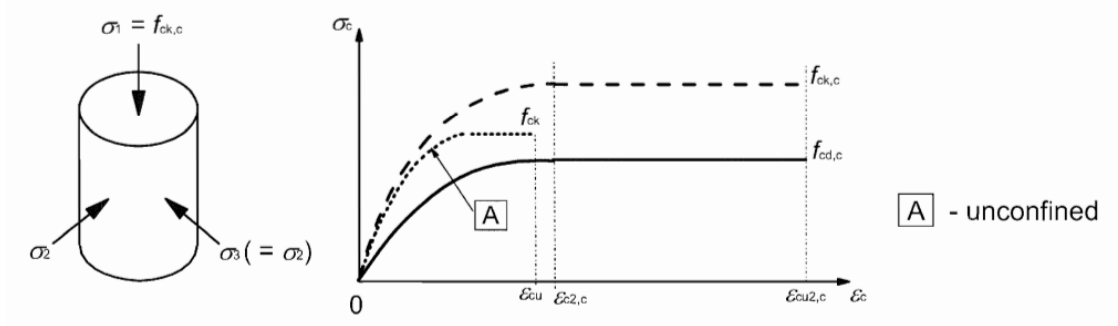


Figure 1.3: Confined concrete behavior [3]

It is also relevant to mention that, as is modeled in equations 1.5 to 1.8, the confinement of concrete doesn't only increase the compressive strength but also the ductility. This is a very important property that is always beneficial in structures due to its contributing to energy dissipation in case of limit situations, as well as making elements easy to monitor for damage. Aside from this, it's important to state that unreinforced, unconfined concrete always displays a brittle failure mechanism, making it an extremely dangerous material to use by itself.

Despite the well-studied mechanical properties of concrete previously mentioned and the wide array of research into them, these can critically change when the material is exposed to high temperatures (as in the case of an accidental fire in the structure). Studies tend to show the following results regarding the main mechanical properties considered for structural design:

- **Compressive Strength**

There is an unavoidable reduction of compressive strength when exposed to higher temperatures, but studies [6] have shown that there are mainly three stages experienced by concrete when heated:

1. Room temperature—300 C, compressive strength of concrete keeps constant or even increases slightly.
2. 300–800 C, compressive strength of concrete decreases dramatically.
3. 800 C afterward, almost all the compressive strength of concrete has been lost.

This can also be observed in the recompilation of studies in figure 1.4, where these three stages can be distinctively recognized.

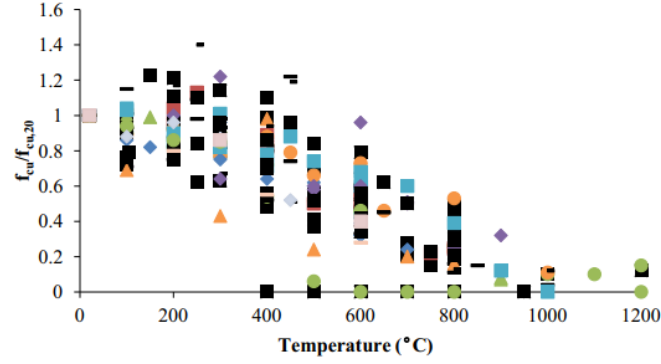


Figure 1.4: Residual compressive strength of concrete at elevated temperatures [6]

- Tensile Strength

It has been observed that the tensile strength decreases linearly as temperature increases, but this study will not deepen in this behavior as the tensile strength is generally neglected for structural design situations.

- Stress-Strain Relationship

Studies regarding this relationship have shown that as the temperature of the material increases, the stress-strain curve tends to become flatter. This means that the peak stress tends to shift downwards and to the right, indicating a decrease in both the compressive strength and the modulus of elasticity. This behavior is shown in figure 1.5. It is also worth noting that the shift to the right also means that the deformations at the peak compressive strength tend to be higher.

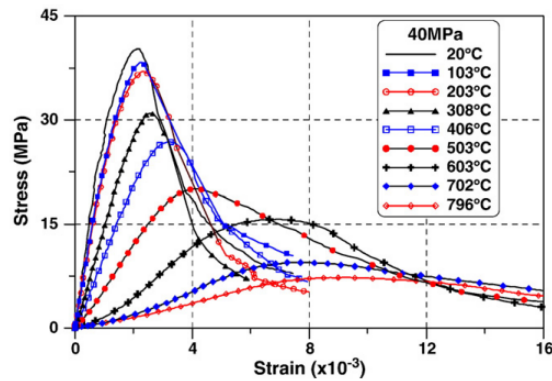


Figure 1.5: Experimental stress-strain curves after heating for different temperatures [7]

- Spalling

Along with the increase in temperature comes a great increase in spalling of concrete. This refers to the "peeling off" of concrete due to the internal thermal stresses and the increased vapor pressure surpassing the available tensile strength of the material [8]. It is also important to mention that spalling has a detrimental effect on any structural element's strength due to the reduction of the resisting cross-section. An example of this situation can be observed in figure 1.6.



Figure 1.6: Example of spalling in a RC beam [9]

Another relevant aspect of spalling is that, in reinforced concrete structures, it exposes or greatly reduces the coverage of steel. Due to steel having a much higher thermal conductivity, a reduced or nonexistent coverage reduces the capacity of the structural element faster in the case of fire.

1.3.2 Steel

Steel is an alloy of iron and carbon with improved mechanical properties over regular iron and is widely used in the construction industry. Unlike concrete, steel presents the same behavior to tensile and compressive stress.

In the case of both reinforcing and structural steel, the most relevant design parameter are its yielding strength f_y , which marks the end of the elastic behavior of the material, and its ultimate strength f_u , which is the highest tension the material can support. These can be observed, as well as the associated deformations, in figure 1.7.

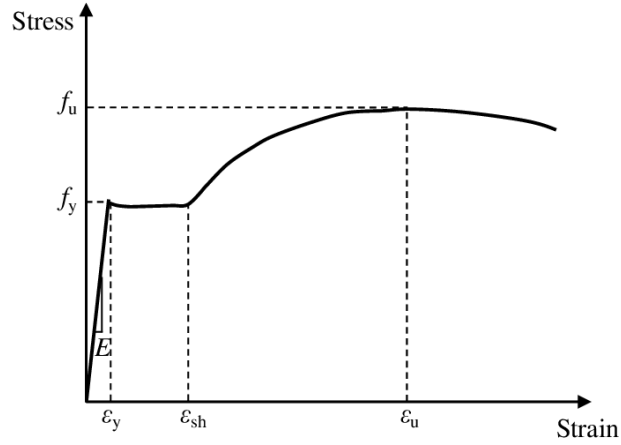


Figure 1.7: Typical stress-strain relationship of hot rolled steel in traction [10]

Analog to the situation for concrete, the yielding stress of reinforcing steel is also reduced from the characteristic strength in the following way:

$$f_{yd} = \frac{f_{yk}}{\gamma_c} \quad (1.9)$$

Where the partial safety factor $\gamma_c = 1,15$ accounts for the more controlled production environment (as in relation to concrete production).

As for the stress-strain relationship of steel, also a simplified model is taken into account. This can follow either one of the curves marked with the letter B in figure 1.8.

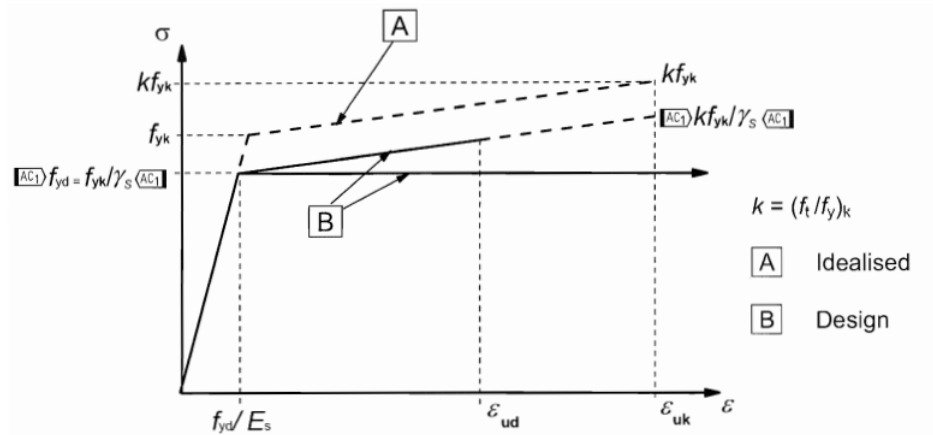


Figure 1.8: Idealised and design stress-strain diagrams for reinforcing steel (for tension and compression)[3]

As for the case of concrete, steel's mechanical properties also depend heavily on the working temperature. A study taking into account cold-formed steel with a structural grade S280 [11] obtained the stress-strain profile at 20, 100, 200, 300, 400, 500, 600, 700, and 800 degrees Celsius, and obtained the results shown in figure 1.9. In this, we can observe that the curves obtained for 100 °C and 200 °C show a decrease in ductility, and in the case of 200 °C even an increase in the ultimate strength. Regardless, the general behavior shows that an increment in temperature results in decreased yielding and ultimate strength as well as an increment in ductility.

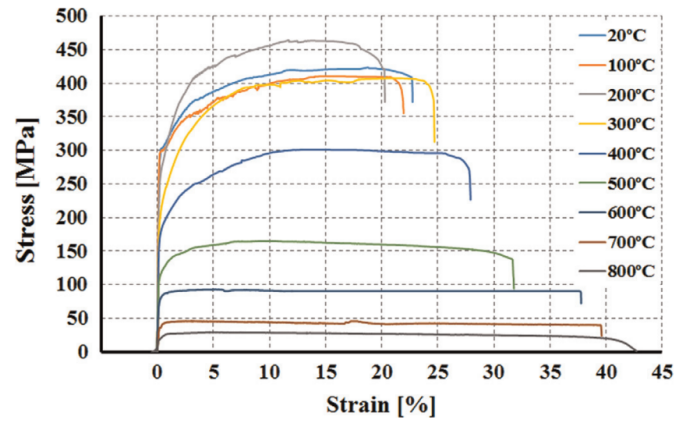


Figure 1.9: Stress-strain curve for steel S280 at different temperatures [11]

More specifically, it can be observed that steel at 700 °C has a yielding strength of about 10% of the yielding steel at room temperature, and at 800 °C of only about 6.5%. Due to this drastic decrease in mechanical properties at higher temperatures, and the fact that steel has a low thermal resistivity, fire resistance design tends to be really important for steel structures.

1.4 Composite Sections

Composite sections are those made up of two or more materials with significantly different mechanical and/or chemical properties that in conjuncture produce a section with different properties to those associated with the base materials by themselves. This is generally done to highlight each material's strengths and mitigate for their weakness, similar to the concept of reinforced concrete.

Some typical cross-sections used for composite columns are shown in figure 1.10.

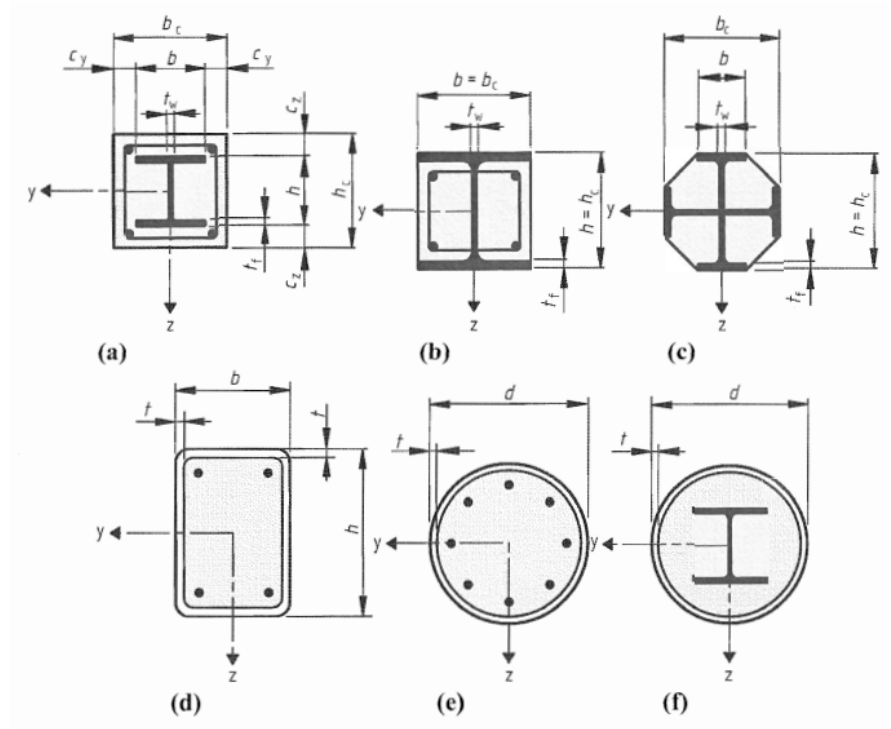


Figure 1.10: Typical cross-sections of composite columns and notation, [12]

In the present study, the focus will be mainly on reinforced concrete-filled hollow steel section (RCFHSS) columns of rectangular shape, which can be observed in figure 1.10 (d). Composite columns present a wide array of advantages born out of the composite behavior of the materials, such as ([13], [14]):

- Reduced cross sections, providing more available floor space for architectural design.
- Great fire and corrosion resistance provided by concrete.
- In the case of concrete-filled steel tubes, the outer steel limits spalling and keeps concrete coverage in place (protection of the inner reinforcement).
- In the case of concrete-filled steel tubes, the need for formwork is eliminated.
- In the case of concrete-filled steel tubes, decreased construction time and costs as a result of prefabrication.
- Drying shrinkage and creep are much smaller in composite members than in ordinary conventional reinforced concrete.

The following is an example to illustrate the structural advantage shown by a RCFHS column in relation to a regular reinforced concrete column of similar dimensions.

For the RC columns, a regular squared section of 40 cm by 40 cm was considered (concrete class C25/30), with a symmetrical reinforcement disposition of $8\phi 26$ with a concrete coverage of 5 cm. These results were computed through the use of the free software Verifica Cemento Armato Stato Limite Ultimo (VcaSlu), and the results are in accordance with those required by Eurocode 2 [3]. The results can be appreciated in figures 1.11 and 1.12.

File Materiali Opzioni Visualizza Progetto Sez. Rett. Sismica Normativa: NTC 2018 ?

TITOLO :

N° Vertici Zoom N° barre Zoom

N°	x [cm]	y [cm]
1	0	0
2	0	40
3	40	40
4	40	0

N°	As [cm²]	x [cm]	y [cm]
1	5,31	5	5
2	5,31	5	20
3	5,31	5	35
4	5,31	20	5
5	5,31	20	35
6	5,31	35	5
7	5,31	35	20
8	5,31	35	35

Sollecitazioni
S.L.U. Metodo n

N_{Ed} kN
M_{xEd} kNm
M_{yEd} kNm

Materiali

B450C C25/30

ϵ_{su} ‰ ϵ_{c2} ‰
f_{yd} N/mm² ϵ_{cu} ‰
E_s N/mm² f_{cd} ‰
E_s/E_c f_{cc}/f_{cd} ?
 ϵ_{syd} ‰ $\sigma_{c,adm}$ N/mm²
 $\sigma_{s,adm}$ N/mm² τ_{co} N/mm²
 τ_{c1} N/mm²

Tipo rottura
Lato calcestruzzo - Acciaio snervato

M_{xRd} kN m
M_{yRd} kN m
 σ_c N/mm²
 σ_s N/mm²
 ϵ_c ‰
 ϵ_s ‰
d cm
x x/d
 δ

Tipo Sezione
☐ Rettan.re ☐ Trapezi
☐ a T ☐ Circolare
☐ Rettangoli ☒ Coord.
☐ DXF

Metodo di calcolo
☒ S.L.U.+ ☐ S.L.U.-
☐ Metodo n

Tipo flessione
☐ Retta ☒ Deviata

N° rett.

Calcola MRd Dominio Mx-My

angolo asse neutro θ°

☐ Precompresso

Figure 1.11: Input parameters and results obtained for a RC column 40x40 with $8\phi 26$ symmetrical reinforcement

As can be seen in figure 1.12, trial actions $M_{x,Ed} = 300$ kNm and $M_{y,Ed} = 200$ kNm were inserted, well outside the resisting interaction domain of the RC column.

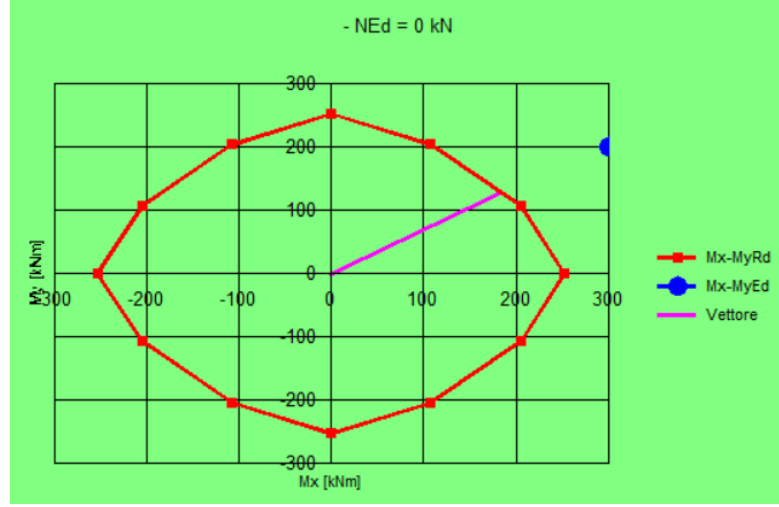


Figure 1.12: $M_x - M_y$ domain, $N = 0$

The simplified approach proposed in section 6.7.3 of Eurocode 4 [12] was taken into consideration for the resistance of the composite columns in the present example. This column was designed to be of the same dimensions as the previous RC column, and so its geometrical dimensions are the following:

- Concrete square of 38 cm by 38 cm.
- Symmetrical reinforcement of $8\phi 26$, with a concrete cover of 5 cm (until the edge of the concrete square).
- Steel squared profile with a thickness of 1 cm encasing the concrete square section.

The result obtained from a cross-section matching this description can be seen in figure 1.13. It is clear that the exact same demanding actions are comfortably inside the resisting domain, and the utilization factor for this section is 0.52. It is also important to mention that the shape of the domain differs from that of a RC column given that section 6.7.3.7 of Eurocode 4 [12] states that the combined compression and biaxial bending resistance of a composite column cross section must be assessed in accordance to 1.10 and 1.11, which provides a conservative approach to the simultaneous action in both main axis.

$$\frac{M_{y,Ed}}{\mu_{dy}M_{pl,y,Rd}} \leq 0.9 \text{ and } \frac{M_{z,Ed}}{\mu_{dz}M_{pl,z,Rd}} \leq 0.9 \quad (1.10)$$

$$\frac{M_{y,Ed}}{\mu_{dy}M_{pl,y,Rd}} + \frac{M_{z,Ed}}{\mu_{dz}M_{pl,z,Rd}} \leq 1 \quad (1.11)$$

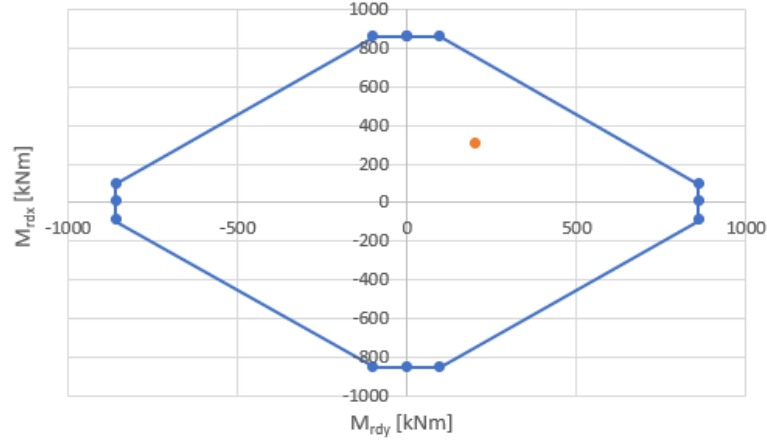


Figure 1.13: $M_x - M_y$ domain of composite section, $N = 0$

As we can see, the resistance provided by the composite cross-section holds a great advantage over a section with the same dimensions and reinforcement but realized with a traditional RC approach. The results obtained for the same experiment but with different steel thicknesses are shown in table 1.2. It should be noted that composite sections with a thickness of less than 10 mm are actually smaller in dimension than the original RC column as the squared concrete section and reinforcements were kept the same as in the original case with $t = 10$.

Column Type	$M_{r,dx}$ [kNm]	$M_{r,dy}$ [kNm]
Comp, $t = 10$	954	954
Comp. $t = 8$	814	814
Comp. $t = 5$	612	612
Comp. $t = 3$	461	461
RC column	252.8	252.8

Table 1.2: Comparative results between columns

From this small exercise it is evident that the composite columns provide higher resistance even with smaller cross sections than RC columns, and as such provide higher structural flexibility and a bigger available space for architectural purposes.

Chapter 2

State of the Art on Fire Resistance Calculation - Composite Columns

The state of the art on this subject is one that is constantly evolving as new research and developments emerge. Some of the key aspects currently investigated by researchers include:

- Creation and verification of numerical models that can precisely forecast the fire performance of composite columns. This entails employing methods such as finite element analysis and computational fluid dynamics to simulate the transfer of heat, structural reaction, and fire-induced damage sustained by composite columns during exposure to fire conditions.
- Studying the effects of different parameters on the fire resistance of this type of column. This encompasses parameters like the steel and concrete types, the column's size and geometry, the thickness of its steel and concrete layers, as well as the environmental exposure conditions.
- The accuracy of the different design methods available. There are several different design methods (Eurocode 4 - part 2 [15] alone proposes three different methods for evaluating composite columns' fire resistance) and research is regularly conducted for future improvements.

In this study, emphasis will be made on some of the main papers and research currently dictating the calculation of fire resistance, as well as the approaches suggested by Eurocode 4.

2.1 Eurocode Approach

The Eurocode 4 - part 2 allows for three different approaches when it comes to evaluating the fire resistance of a composite column:

- Recognized design solutions called tabulated data for specific types of structural members.
- Simple calculation models for specific types of structural members.
- Advanced calculation models for simulating the behavior of the global structure, of parts of the structure, or only of a structural member.

Logically, the simpler methods tend to be more on the side of safety, regularly yielding conservative results.

2.1.1 Tabular Method

The tabular method relies on the utilization of a table (visible in figure 2.1) for the estimation of the fire resistance of concrete-filled hollow section columns. This is the most conservative approach provided by Eurocode and as such it is hard to certify a high standard of fire resistance through it. A few considerations regarding this method for concrete-filled composite columns:

- The load level for fire design $\eta_{fi,t}$ can be calculated as:

$$\eta_{fi,t} = \frac{E_{fi,d,t}}{R_d}$$

Where $E_{fi,d,t}$ is the design effect of actions in the fire situation at time t and R_d is the design resistance for normal temperature design.

- The results provided are only valid for standard fire exposure.
- Valid for braced frames.
- Load levels are defined by assuming pin-ended supports of the column for the calculation of R_d , provided that both column ends are rotationally restrained in the fire situation.
- R_d should be based on twice the buckling length used in the fire design situation.
- Valid for columns with a maximum length of 30 times the minimum external dimension of the cross-section chosen.

- When calculating R_d :
 - Irrespective of the steel grade of the hollow sections, a nominal yield point of 235 N/mm² is taken into account;
 - The wall thickness e of the hollow section is considered up to a maximum of 1/25 of b or d ;
 - Reinforcement ratios $A_s / (A_c + A_s)$ higher than 3 % are not taken into account;
 - The concrete strength is considered as for normal temperature design

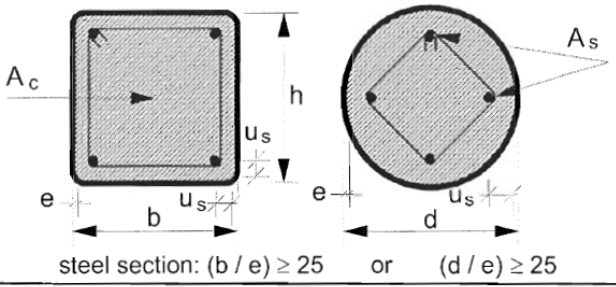
 steel section: $(b / e) \geq 25$ or $(d / e) \geq 25$		Standard Fire Resistance				
		R30	R60	R90	R120	R180
1	Minimum cross-sectional dimensions for load level $\eta_{fi,t} \leq 0,28$					
1.1	Minimum dimensions h and b or minimum diameter d [mm]	160	200	220	260	400
1.2	Minimum ratio of reinforcement $A_s / (A_c + A_s)$ in (%)	0	1,5	3,0	6,0	6,0
1.3	Minimum axis distance of reinforcing bars u_s [mm]	-	30	40	50	60
2	Minimum cross-sectional dimensions for load level $\eta_{fi,t} \leq 0,47$					
2.1	Minimum dimensions h and b or minimum diameter d [mm]	260	260	400	450	500
2.2	Minimum ratio of reinforcement $A_s / (A_c + A_s)$ in (%)	0	3,0	6,0	6,0	6,0
2.3	Minimum axis distance of reinforcing bars u_s [mm]	-	30	40	50	60
3	Minimum cross-sectional dimensions for load level $\eta_{fi,t} \leq 0,66$					
3.1	Minimum dimensions h and b or minimum diameter d [mm]	260	450	550	-	-
3.2	Minimum ratio of reinforcement $A_s / (A_c + A_s)$ in (%)	3,0	6,0	6,0	-	-
3.3	Minimum axis distance of reinforcing bars u_s [mm]	25	30	40	-	-

Figure 2.1: Table 4.7 of EC4, part 1-2 [15], tabular method for establishing fire resistance of concrete-filled hollow section columns.

2.1.2 Simple Calculation Model

The simple calculation models shall only be used for columns in braced frames (same condition as the previous method). The design value in the fire situation, of

the resistance of composite columns in axial compression (buckling load) should be obtained from equation 2.1.

$$N_{fi,Rd} = \chi N_{fi,pl,Rd} \quad (2.1)$$

Where χ is the reduction coefficient for buckling curve c of 6.3.1 of Eurocode 3 [16] and depending on the relative slenderness $\bar{\lambda}_\theta$ and $N_{fi,pl,Rd}$ is the design value of the plastic resistance to axial compression in the fire situation.

The design value of the plastic resistance to axial compression in the fire situation is given by:

$$N_{fi,pl,Rd} = \sum_j A_{a,\theta} f_{ay,\theta} / \gamma_{M,fi,a} + \sum_k A_{s,\theta} f_{sy,\theta} / \gamma_{M,fi,s} + \sum_m A_{c,\theta} f_{c,\theta} / \gamma_{M,fi,c} \quad (2.2)$$

Where the sub-index "a" refers to the steel profile, "s" refers to the steel rebars, and "c" refers to the concrete section. The effective flexural stiffness can then be calculated as:

$$EI_{fi,eff} = \sum_j \phi_{a,\theta} E_{a,\theta} I_{a,\theta} + \sum_k \phi_{s,\theta} E_{s,\theta} I_{s,\theta} + \sum_m \phi_{c,\theta} E_{c,sec,\theta} I_{c,\theta} \quad (2.3)$$

With $\phi_{i,\theta}$ being the reduction coefficient depending on thermal stresses.

The Euler buckling load or elastic critical load in the fire situation can then be calculated as:

$$N_{fi,cr} = \frac{\pi^2 EI_{fi,eff}}{l_\theta^2} \quad (2.4)$$

Where l_θ is the buckling length of the column in the fire situation. The relative slenderness is then given by:

$$\bar{\lambda}_\theta = \sqrt{\frac{N_{fi,pl,R}}{N_{fi,cr}}} \quad (2.5)$$

It should be taken into account that $N_{fi,pl,R}$ is the value of $N_{fi,pl,Rd}$ when the safety factors for the materials are taken as 1. For the determination of the buckling load, the rules of Eurocode 3 [16] apply, with the exception that a column at the level under consideration, fully connected to the column above and below, may be considered as effectively restrained at such connections. This can only be considered provided the resistance to fire of the building elements, which separate the levels under consideration, is at least equal to the fire resistance of the column.

In the particular case of protected concrete-filled hollow sections, a further simplification is suggested and the load-bearing criterion "R" may be assumed to be met provided the temperature of the hollow section is lower than 350°C at that time.

2.1.3 Advanced Calculation Model

The advanced calculation model proposed by Eurocode 4 is not quite a model but rather describes the minimum requirements that an analytical model itself should satisfy in order to be used for this purpose. Eurocode 4 [12] states:

- Advanced calculation models shall provide a realistic analysis of structures exposed to fire. They shall be based on fundamental physical behavior in such a way as to lead to a reliable approximation of the expected behavior of the relevant structural component under fire conditions (these approximations are better than the ones provided by the previous method and lead to a more accurate design).
- Advanced calculation models may be used with any type of cross-section.
- This type of model may include separate calculation models for the determination of the development and distribution of the temperature within structural elements and the mechanical behavior of the structure or of any part of it.

These models can be separated into two parts, as previously mentioned:

- **Thermal Response**
The thermal response shall be based on the acknowledged principles and assumptions of the theory of heat transfer. It shall consider the relevant thermal actions specified in Eurocode 1 [1] and the variation of the thermal properties of the material according to Eurocode 4, part 2 [15]. It also states that the effect of non-uniform thermal exposure may be considered, as well as the fact that the influence of moisture content may be conservatively neglected.
- **Mechanical Response**
The mechanical response shall be based on the acknowledged principles and assumptions of the theory of structural mechanics, taking into account the effects of temperature. It shall also take into account the combined effect of mechanical actions, geometrical imperfections, and thermal actions, the temperature-dependent mechanical properties of the materials, geometrical non-linear effects, and the effects of non-linear material properties, including the effects of unloading on the structural stiffness. The effects of all thermally induced strains and stresses also need to be accounted for. Finally, the

deformation at the ultimate limit state should also be limited as necessary to ensure that compatibility is maintained between all parts of the structure.

The validity of all advanced calculation models should be verified with relevant test results and should be accompanied by a sensitivity analysis (considering critical parameters, such as buckling length, element size, load level, etc.) to ensure that the model complies with sound engineering principles.

2.2 Current Research and Proposed Models

2.2.1 "Fire Resistance of Rectangular Steel Columns Filled with Bar-Reinforced Concrete" by T.T. Lie and R.J. Irwin [17]

This study focused on the development of a mathematical model to calculate the temperatures, deformations, and fire resistance of rectangular steel columns filled with bar-reinforced concrete, and compared those results with the ones measured experimentally. This model allows for the evaluation of the critical parameters for these kinds of columns, such as the load, column section dimensions, column length, percentage of reinforcing steel, etc.

Thermal Response

Column temperatures are calculated by a finite-difference method. This consists in many different steps, which will be described below:

- **Division of Cross Section into Elements**

The composite column's cross-sectional area is divided into square and triangular elements arranged in a triangular network. The elements are square inside the steel and concrete, and triangular at the column surface and along the boundary between the concrete and steel. The temperature at the center is used to represent the square elements, and representative points are located at the center of each hypotenuse for the triangular elements. Only one-quarter of the section is considered for symmetry reasons (it is assumed that fire exposure is even along all sides). This subdivision can be seen in figure 2.2.

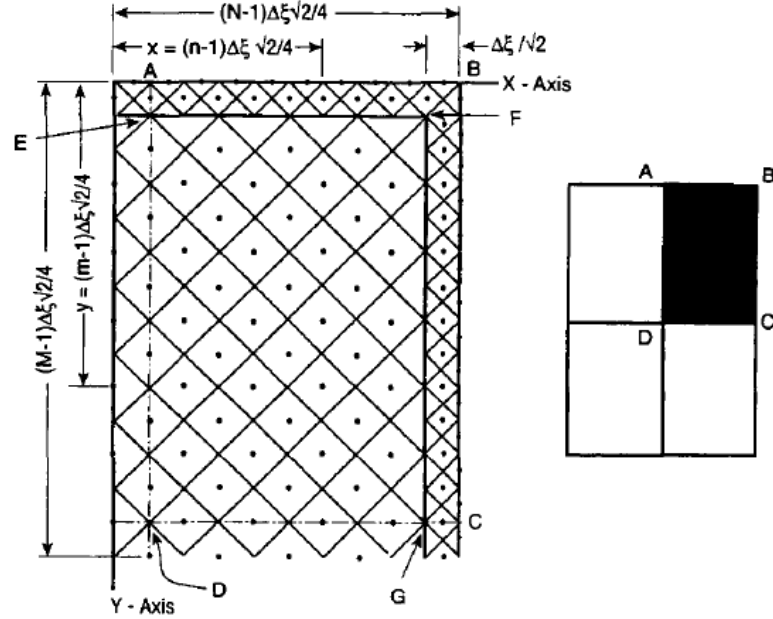


Figure 2.2: Thermal network in quarter section [17]

- Equations for Temperature Transference For this particular study, the temperature course was considered as in ASTM E119 [18], and can be approximately described by the following expression:

$$T_t = 20 + 750(1 - \exp(-3.79553\sqrt{t})) + 170.41\sqrt{t} \quad (2.6)$$

Where t is the time in hours and T_t is the fire temperature in °C. The full detail of the temperature transference equations will not be discussed in this study as they are described extensively in the original study ([17]), but they are defined for each of the 4 different boundaries found in the model:

1. Transference at fire-steel boundary
2. Transference inside the steel
3. Transference at steel-concrete boundary
4. Transference inside the concrete

Additionally, auxiliary equations are used to account for the symmetry assumption previously made. The effect of moisture is also taken into account, considering that all the heat received by an element once it has reached 100°C is used for water evaporation until it is dry.

With the help of all these equations and the relevant thermal properties of these materials, the temperatures in the column and on its surface can be calculated for any time $t = (j+1)\Delta t$ if the temperature distribution at the time $j\Delta t$ is known. Starting from an initial temperature of 20°C, the temperature history of the column can be calculated by the repeated application of these equations.

Mechanical Response

The calculation of the strength of the column exposed to fire was achieved through load deflection analysis. The method assumes that the columns being tested are pin-ended and have a length of KL . Although there is a small eccentricity due to imperfections, it is assumed to be negligible in the calculations. The initial eccentricity is assumed to be 0.2 mm, as it has been found that an eccentricity of up to 3 mm has a small effect on fire resistance. A finite value for the initial eccentricity is selected to enable the computer program to work. The curvature of the column is assumed to vary from pin end to mid-height according to a straight-line relation, as illustrated in fig. 2.3.

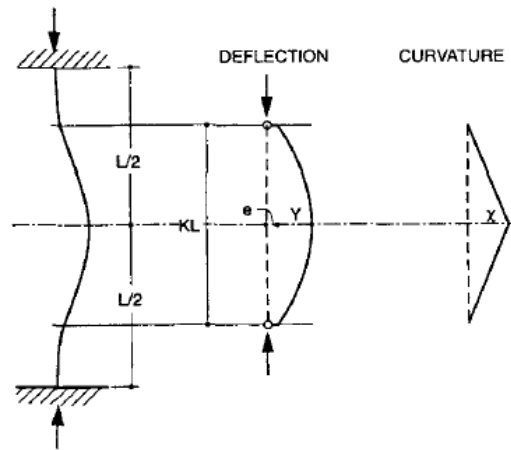


Figure 2.3: Load-Deflection Analysis [17]

For any given curvature, and for any given deflection at mid-height, the axial strain is varied until the internal moment at the midsection is in equilibrium with the applied moment. The load-deflection curve can be calculated at different times during the exposure to fire to determine the column's strength, which is the maximum load it can carry. The following assumptions are made in the calculation of column strength:

1. The properties of the concrete and steel are those described in Appendix I of

the original study [17].

2. Concrete has no tensile strength.
3. Plane sections remain plane.
4. No slip between materials.
5. No composite action between the steel and the concrete.
6. The reduction of column length before exposure to fire is negligible (creep, shortening because of load, etc.).

The resistance of the column can then be obtained through the sum of the loads carried by each element and the moments contributed by them. These are calculated for each element through their respective stress-strain relationships and considering the total strains as given by the sum of the thermal expansion strain, the strains due to axial load, and the strains resulting from the bending of the column.

Results

The thermal response yielded the results available in figures 2.4 to 2.6. These figures show the difference in temperature calculated and measured along the center line of each column. The results tend to be in good agreement, but some discrepancies can be observed. This may be due to the fact that the model only takes into account the evaporation of moisture and not the migration of moisture, which refers to the thermally induced movement of moisture toward the cooler center of the column.

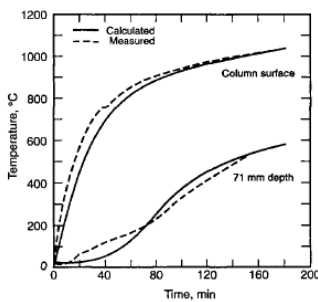


Figure 2.4: Temperature along Center line of Column (203 x 203 x 6.35 mm)

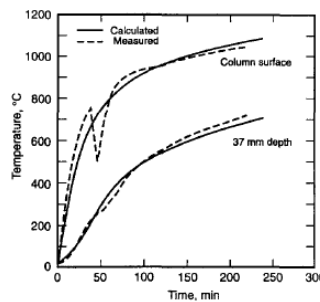


Figure 2.5: Temperature along Center line of Column (305 x 305 x 6.35 mm)

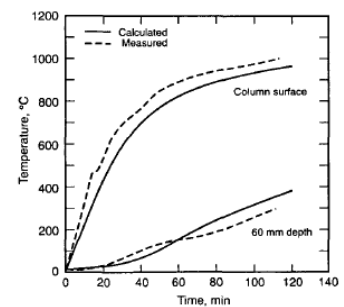


Figure 2.6: Temperature along Center line of Column (254 x 254 x 6.35 mm)

The mechanical response model yielded the results displayed in figures 2.7 to 2.10. Figures 2.7 to 2.9 show the results obtained for the axial deformation (measured and calculated) as a function of time. There is a good agreement in the trend displayed by the calculated and measured axial deformations, however, there are some differences between the values. The axial deformation depends on several factors, and given the dimensions in consideration (deformations in the order of 20 mm for a column with a length of 3800 mm), a small discrepancy in any of these factors could produce the margin of error observed. As for figure 2.10, we can observe that there is a generally good agreement between the results obtained for columns 2 and 3, but the difference in fire resistance calculated and measured for column 1 is 30%. This is a considerable difference, however, due to it being on the conservative side, it can be considered acceptable.

2.2.2 "Fire Resistance of Steel Columns Filled with Bar-Reinforced Concrete" by T.T. Lie and V. K. R. Kodur [19]

This study realized a parametric study, using mathematical models, to establish the influence of various factors in the fire resistance capacity of steel columns (rectangular and circular) filled with bar-reinforced concrete. Data obtained through these studies were then used to develop simple expressions that allow for calculating the fire resistance of these columns.

Through these studies, the parameters that were found to be the most determinant were:

- **Outside Diameter or Width of the Column**
It was found that the fire resistance increases more than quadratically with the column outside diameter. The composite column's increased fire resistance can be attributed mostly due to two factors: the increase in strength with diameter/width (higher supporting section) and the concrete core taking longer to reach temperatures high enough so it can no longer support the load applied.
- **Steel Wall Thickness**
It was studied that for larger columns, the fire resistance decreases slightly with wall thickness while, for smaller columns, it increases slightly. The explanation suggested consists of the fact that bigger columns fail after longer exposure than smaller columns. In this sense, the steel holds nearly no mechanical properties at the time of failure of bigger columns. However, small columns tend to fail after a reduced time exposure to fire, and as such the steel still contributes considerably to the load-bearing capacities of the column.

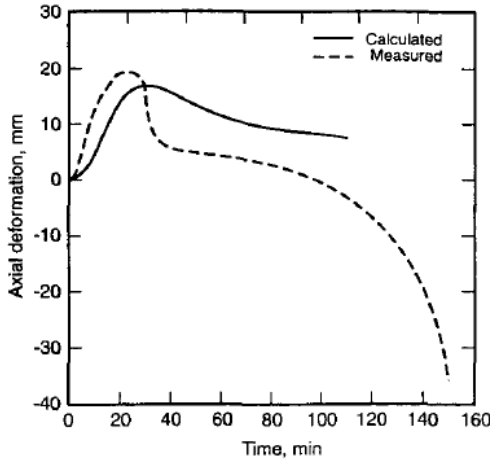


Figure 2.7: Calculated and Measured Axial Deformations of Column (203 x 203 x 6.35 mm)

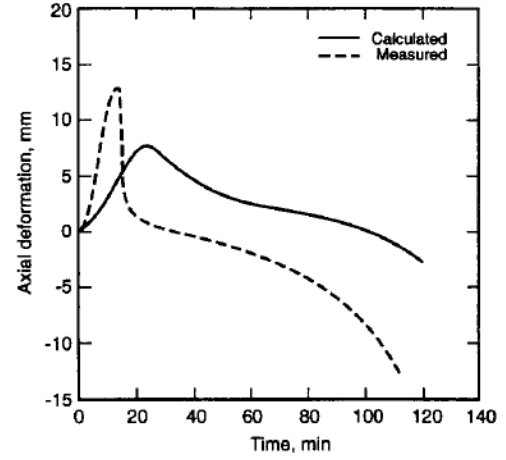


Figure 2.8: Calculated and Measured Axial Deformations of Column (254 x 254 x 6.35 mm)

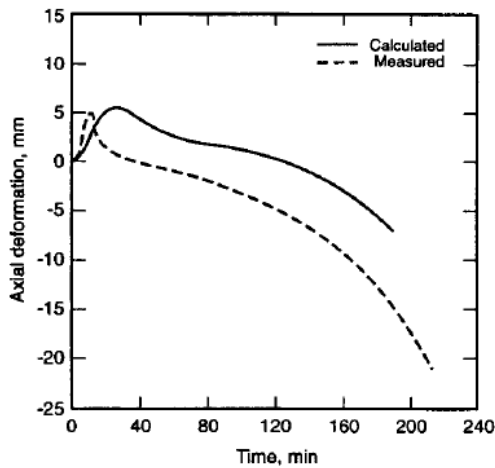


Figure 2.9: Calculated and Measured Axial Deformations of Column (305 x 305 x 6.35 mm)

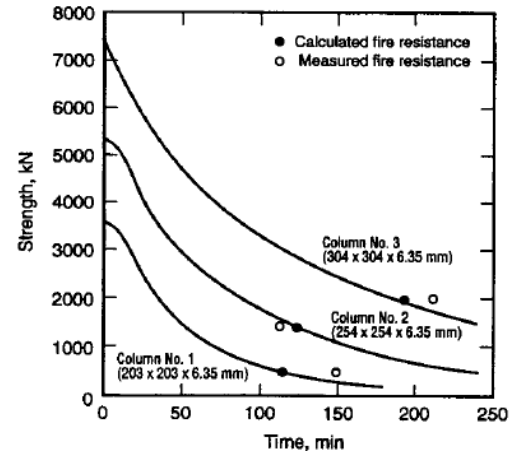


Figure 2.10: Calculated Column Strengths as Function of Time and Calculated Measured Fire Resistance

- Effective Length

As could be expected, results showed that fire resistance decreases along with the increment in effective length. Furthermore, it was observed that the influence of this parameter is greater for lower loads.

- Load

It was observed that, for all the columns modeled, fire resistance decreases steeply with increments in the load applied.

- Percentages of Steel Reinforcements

The parametric studies showed that the increment in fire resistance obtained by increasing the percentage of steel reinforcement is relatively small. This was around 10% when increasing the steel percentage from 1.5% to 6%. However, it was noted that the presence of reinforcement still substantially increases the fire resistance when compared with steel columns filled with plain concrete.

- Concrete Strength

The fire resistance of the column is moderately influenced by the concrete strength. It was observed that fire resistance increases almost linearly with the concrete strength. The influence was also noted to be greater for higher loads and shorter columns.

- Concrete Cover

As could be expected (and is regularly contemplated in different structural design codes), fire resistance showed to increase along with the increment in concrete cover. This is well documented to be due to the thicker concrete cover slowing the temperature propagation to the inside reinforcement bars, thus allowing them to keep higher mechanical properties for extended periods.

- Type of Aggregate

HSS columns filled with bar-reinforced carbonate aggregate concrete showed a higher fire resistance of 10% or more than those filled with siliceous aggregate concrete. This is mainly due to the higher heat capacity of carbonate aggregate concrete.

Expressions for Calculating Fire Resistance

Using the results of the studies on fire resistance and related parameters, an empirical formula was developed to calculate the fire resistance of hollow steel columns filled with bar-reinforced concrete. This formula takes into account the 7 most relevant parameters found in these studies (diameter/width of the column, load, effective length, concrete strength, type of aggregate, percentage of reinforcing steel and concrete cover), and proposes the following empirically established formula:

$$R = f \frac{(f'_c + 20)}{(KL - 1,000)} D^2 \sqrt{\frac{D}{C}} \quad (2.7)$$

Where R refers to the fire resistance in minutes; f'_c is the specified 28-day concrete strength in MPa; K is the effective length factor; L is the unsupported

length of the column in mm; D is the outside diameter/width of the column in mm; C is the service load in kN; and finally, f is a constant that takes into account the type of aggregate, percentage of steel reinforcement, and the thickness of the concrete cover. Table 2.1 shows the different values that this constant can take depending on the previously mentioned parameter. In this, f_1 refers to the constant for circular columns, while f_2 should be applied for square columns.

Aggregate Type (1)	Percentage steel reinforcement (2)	Concrete cover thickness (mm) (3)	Values of f_1 (4)	Values of f_2 (5)
Siliceous	<3%	<25	0.075	0.065
Siliceous	<3%	≥ 25	0.08	0.07
Siliceous	$\geq 3\%$	<25	0.08	0.07
Siliceous	$\geq 3\%$	≥ 25	0.085	0.075
Carbonate	<3%	<25	0.085	0.075
Carbonate	<3%	≥ 25	0.09	0.08
Carbonate	$\geq 3\%$	<25	0.09	0.08
Carbonate	$\geq 3\%$	≥ 25	0.095	0.085

Table 2.1: Values of f_1 and f_2

Given that the parametric study is limited in the range studied for each parameter, so is the range in which equation 2.7 should be considered valid. The following limits were set:

1. Fire resistance (R) ≤ 180 min
2. Load on the column (C) ≤ 1.7 times the factored compressive resistance of the concrete core
3. Specified 28-day concrete compressive strength (f'_c) 20-55 MPa
4. Effective length of the column (KL) 2000-4500 mm
5. Outside diameter/width 175-305 mm
6. Percentage of main reinforcing bars 1.5% to 5%
7. Concrete cover 20-50 mm
8. Width to thickness ratio of steel profile not to exceed class section 3 in accordance with CAN/CSA-S.16.1-M89 [20].

Results

Equation 2.7 was obtained through approximation and linearization of a series of different parameters in order to keep the formula simple. Due to this, the aim was in obtaining an expression that results in somewhat conservative resistance. Figure 2.11 shows the comparison between the results obtained through the use of equation 2.7 and tests results obtained from different studies ([21], [22]). It is clear that there are big differences between calculated and experimental values. Even nominally identical columns tested at different laboratories have been proved to show significant differences in fire resistance and this is mainly attributed to variations in end fixity of the different testing machines. However, there is some degree of correspondence with the equation yielding regularly conservative results.

On the other hand, we can see in figure 2.12 that the results produced through this method tend to be slightly more conservative than those coming from the program model previously described. Regardless, both methods produce, in most cases, conservative fire resistances in comparison with test results.

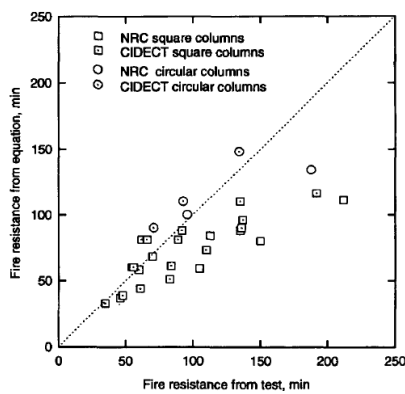


Figure 2.11: Comparison of Calculated Fire Resistance with That from Tests

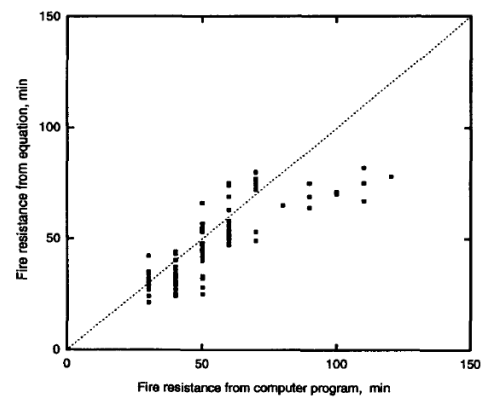


Figure 2.12: Comparison of Fire Resistance for Square HSS Columns with Model Predictions

2.2.3 "Enhancing the Fire Performance of Concrete-Filled Steel Columns through System-Level Analysis" by R. S. Fike and V. K. R. Kodur [23]

This study builds on the models and empirical formulas proposed previously and furthermore states that the actual resistance of these types of columns can be estimated more accurately through the use of system-level analysis.

There has been a push towards a fire safety design approach based on performance, mainly due to the fact that the current approaches are limited and restrictive. The performance-based design offers two ways to improve this. One is to test a representative structure under fire conditions, while the other is to use computer simulations to model a realistic fire. Testing is highly limited due to the elevated price, and so it's usually only done to check the accuracy of computer models. Furthermore, using computer models allows for consideration of the most significant factors that affect fire resistance. The key factors that differ from the current approach in the standards are:

- Fire Scenario

While standard fire curves such as those proposed by ASTM E-119 [18] or ISO 834 [24] are useful to establish the relative performance of columns, they are not truly representative of the conditions in a fire and cannot be relied upon for the determination of the time resistance of a composite column in a fire. In this sense, the standard fire curves tend to overestimate the temperature conditions. A study [25] studied the decay phase of realistic fire scenarios, which can be observed in figure 2.13. During this decay phase, the cross-section of the column enters a cooling phase during which the materials recover part of their strength and stiffness, increasing fire resistance.

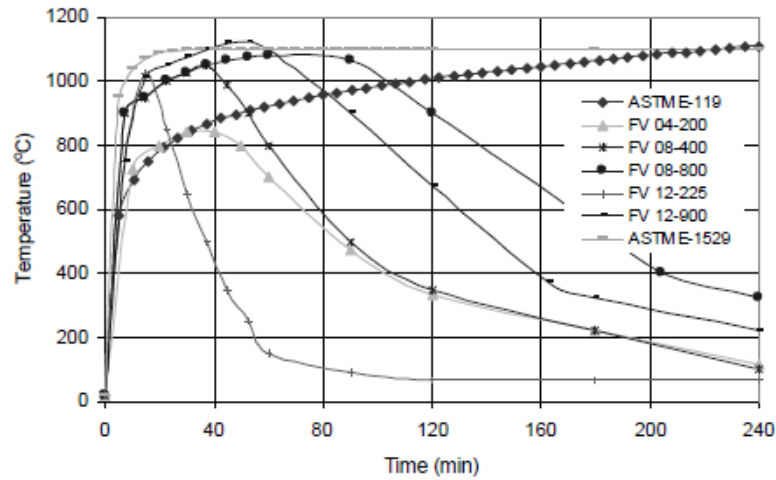


Figure 2.13: Time-temperature relationship for various fire scenarios [Kmag]

- Load Level

Fire resistance is evaluated through standard fire tests using codes of practice that usually consider a load ratio of approximately 50%. In real-life scenarios, this ratio is influenced by various factors such as occupancy type, dead load

to live load ratio, and safety factors used in design for both normal and fire conditions. The load ratio might be an influential parameter in the fire resistance calculation, and as such should be taken into account more accurately.

- **Member Interactions**

Fire resistance testing and numerical simulations are highly complex in order to account for the thermo-mechanical loading of the columns. Due to this, they often only consider a single structural member exposed to fire. This doesn't account for how the member interacts with other parts of the structure, which can help redistribute loads and limit temperature in critical areas. To accurately predict fire resistance, it is necessary to consider these interactions and move towards a performance-based approach.

- **Failure Criterion**

When testing the ability of a structure to resist fire, a temperature limit of 538°C is commonly used to define failure. However, this does not take into account the effect of the concrete core. The stability of the column under fire conditions must be considered, as it can fail due to buckling or crushing, which can happen even after the temperature limit is reached. If a column is fixed at both ends, the redistribution of moments can enhance its fire resistance. Additionally, local stability should be considered as the column can fail due to crushing or buckling of the steel wall.

Based on these appreciations, numerical studies were carried out to evaluate the fire resistance of concrete-filled hollow steel section columns exposed to various different fire and loading scenarios through a system-level approach. For this purpose, the finite element-based computer program SAFIR was utilized and the building under investigation was an eight-story steel-framed building.

The study analyzed 11 different fire scenarios, column configurations, and floor slab types to understand the performance of the structural frame under fire conditions. The first case was analyzed without fire protection on the columns or secondary beams, and then the second contemplated the replacement of columns using CFHSS sections. The remaining cases replaced the columns and floor system with CFHSS columns and SFRC (steel fiber reinforced concrete) floor systems designed according to AISC provisions. One and three-story models were tested to assess the structure's response to fire exposure. The results of the analyses are presented in Table 2.2.

	Fire Exposure	# of Stories Under Fire	Column Type	Floor Slab Configuration	Fire Resistance (min)	Failure Zone Member
C-1	ASTM E-119	1	W-Shape	Plain Concrete	16.5	W-col.
C-2	ASTM E-119	1	CFHSS	Plain Concrete	58	slab
C-3	ASTM E-119	1	CFHSS	SFRC	118	slab
C-4	Extreme	1	CFHSS	SFRC	12.5	slab
C-5	Extreme	3	CFHSS	SFRC	13	slab
C-6	Severe	1	CFHSS	SFRC	37	slab
C-7	Severe	3	CFHSS	SFRC	39	slab
C-8	Medium	1	CFHSS	SFRC	No failure	None
C-9	Mild	1	CFHSS	SFRC	No failure	None
C-10	Medium	3	CFHSS	SFRC	No failure	None
C-11	Mild	3	CFHSS	SFRC	No failure	None

Table 2.2: Various structural configurations and fire scenarios simulated in the building [23], adapted.

Conclusions

This study showed that using CFHSS columns in composite construction can significantly improve the fire resistance of structural steel framing. By considering realistic loading, fire exposure, failure criterion, and member interactions through system-level analysis, the fire resistance of CFHSS columns can be significantly improved. The study suggests that in steel-framed office buildings, external fire protection to columns may not be necessary if composite construction using CFHSS columns is implemented. Additionally, the study found that concrete-filled steel columns can withstand two hours of standard fire exposure or complete burnout of medium or less severe design fires without any fire protection.

2.2.4 "Fire resistance of restrained composite columns made of concrete filled hollow sections" by João Paulo C. Rodrigues and Luís Laím [26]

This study decided to focus on a different parameter than those generally investigated for concrete-filled hollow sections, and aims at characterizing the influence of the axial and rotational restraint on the buckling behavior of these columns in case of fire. With this as the main objective, the test parameters chosen were: column slenderness, type of cross-section, and axial and rotational restraining of

the surrounding structure to the testing columns.

In this way, the test plan observable in table 2.3 shows the parameters associated to the different columns tested.

Test reference	A (mm ²)	R	$N_{pl,Rd}$ (kN)	N_{cr} (kN)	$N_{b,Rd}$ (kN)	$k_{a,c}$ (kN/mm)	$k_{r,c}$ (kNm/rad)	P_o (kN)	k_a (kN/mm)	k_r (kNm/rad)
CC273-30 ka	58535	0.41	4016	26416	3814	1094	24695	1144	30	94615
SC220-30 ka	48400	0.44	3987	21967	3751	1005	20528	1125	30	94615
CC194-30 ka	29468	0.58	2178	7097	1956	573	6632	587	30	94615
RC350-30 ka	52500	0.61	4385	12549	3880	1104	11727	1164	30	94615
RC250-30 ka	37500	0.63	3436	9258	3016	837	8651	905	30	94615
SC150-30 ka	22500	0.65	2043	5158	1776	500	4820	533	30	94615
EC320-30 ka	40212	0.69	4118	9216	3248	965	8612	974	30	94615
CC273-110 ka	58535	0.41	4016	26416	3814	1094	24695	1144	110	131340
scno-110 ka	48400	0.44	3987	21967	3751	1005	20528	1125	110	131340
CC194-110 ka	29468	0.58	2178	7097	1956	573	6632	587	110	131340
RC350-110 ka	52500	0.61	4385	12549	3880	1104	11727	1164	110	131340
RC250-110 ka	37500	0.63	3436	9258	3016	837	8651	905	110	131340
SC150-110 ka	22500	0.65	2043	5158	1776	500	4820	533	110	131340
EC320-110 ka	40212	0.69	4118	9216	3248	965	8612	974	110	131340

Table 2.3: Test plan of [26]

Where k_r is the rotational restraint and k_a is the axial restraint.

Four different types of cross-sections were studied:

- Circular - 2 cross sections, with diameters of 273 and 193.7 mm. The wider section was reinforced with 8 longitudinal rebars: 4 ϕ 16 and 4 ϕ 10, and a steel tube with a thickness of 10 mm. The narrower section, instead, was reinforced with 4 longitudinal rebars: 4 ϕ 12, and a steel tube with a thickness of 8 mm.
- Square - 2 cross sections, with sides 220 and 150 mm. The wider section was reinforced with 8 longitudinal rebars: 4 ϕ 16 and 4 ϕ 10, and a steel tube with a thickness of 10 mm. The narrower section, instead, was reinforced with 4 longitudinal rebars: 4 ϕ 12, and a steel tube with a thickness of 8 mm.
- Rectangular - 2 cross sections, one 150x350 mm and the other 105x250 mm. The wider section was reinforced with 4 ϕ 16 + 2 ϕ 10, while the narrower section was reinforced only with 4 ϕ 16. Both sections were built with a steel tube with a thickness of 10 mm.
- Elliptical - 1 cross section, 320 mm long by 160 mm wide. The longitudinal reinforcement was 4 ϕ 20, and the steel tube was of a thickness of 12.5 mm.

The detailed position of reinforcing bars can be observed in figure 2.14. All specimens were realized with a similar concrete class C25/30 with calcareous aggregate, steel profiles made of S355 structural steel, and transversal reinforcement of 8 mm diameter stirrups with a spacing of 150 mm until about 800 mm from the end-supports, and with a spacing of 200 mm in the central part. The concrete cover was also kept the same for all test specimens, at 25 mm.

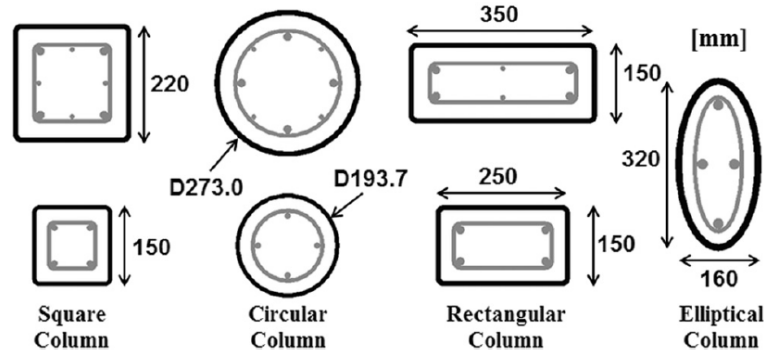


Figure 2.14: Scheme of the cross-sections of the tested columns [26]

The specimens described were then subjected to fire simulation inside a furnace, trying to mimic as well as possible the standard ISO834 curve [24].

Results

This study found that the stiffness of the surrounding structure doesn't have a big impact on the fire resistance of semi-rigid ended columns. Even when the axial and rotational restraint increased significantly (from 30 to 110 kN/mm and 94615 to 131340 kNm/rad, respectively), the fire resistance of the columns only decreased by an average of 5%.

It was found that the most determining factor out of those studied was the shape of the column, with elliptical columns being able to resist 30% longer than squared columns when exposed to the same load level (30%).

The last parameter controlled in this study, the slenderness, also proved to be highly influential on the fire resistance of the columns. When the non-dimensional slenderness increased from 0.44 to 0.65, the time resistance of the columns decreased by 25%.

Finally, the results obtained were also compared with those yielded by the simplified calculation method for fire design of concrete-filled hollows sections exposed to fire all around the column according to the standard temperature-time curve, established in Annex H of Eurocode 4, part 2 [15], and it was found that this produced generally unsafe results.

2.2.5 Other Studies

A wide array of other studies have been conducted in order to assess more accurately the effect of different parameters in the fire resistance of concrete-filled tubular steel sections and develop new predictive models (such as [27], [28], [29], [30], [31], [32], among others). These studies have provided valuable information and should be considered for understanding the behavior of this kind of columns in general, however, the focus of these has been on circular or plain concrete-filled columns, and as such they will not be discussed in detail in this study.

Chapter 3

Mechanical Analysis Tool

3.1 Thermal Response Through CDM Dolmen

As mentioned previously, the analysis will be based on the thermal results obtained from CDM DOLMEN.

CDM DOLMEN is a company born out of engineers who graduated from PoliTo and focuses on the development of software for commercial use in the context of geotechnical and structural engineering. One of the many modules developed by this company is "IS Fuoco", a software for the design and verification of different sections under fire conditions. This program allows for the definition of a cross-section in any of the available materials (or custom-made materials with properties chosen by the user), as well as the definition of the fire exposure on its sides. An example of section and materials definition can be observed in figure 3.1, where the same section as considered in the introduction example was used.

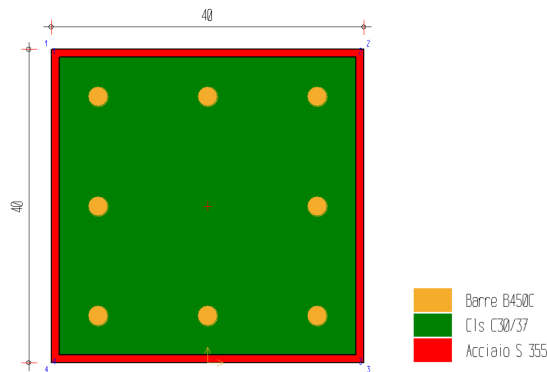


Figure 3.1: Section and materials defined in IS Fuoco

After the geometry and materials have been defined, it is necessary to define the fire exposure. In this case, the general case of fire (as defined by the ISO834 curve [24]) was used and applied on all sides of the column. After this is done, the program generates a mesh and develops a finite element analysis. The analysis can be done in multiple time steps and reports the heat distribution through the section at each of them. In this case, the exposure was considered to be for 120 minutes, with time steps reporting the distribution every 30 minutes.

This program works by solving Fourier's Law equation of heat transfer, which states that:

$$q = -k \frac{dT}{dx} \quad (3.1)$$

where q is the heat flux (rate of heat transfer over the cross-sectional area), k is the thermal conductivity of the materials and dT/dx is the temperature gradient in the direction of transfer [33]. This equation is integrated over time and space for the whole section, taking into consideration the boundary conditions provided by the material borders as well as those in contact with the fire.

The results obtained for the previously mentioned section can be observed from figure 3.2 to figure 3.5. As can be expected, the heat distribution shows that the outside of the section increases its temperature faster, with the corners, in particular, being the part of the section at the highest temperature.

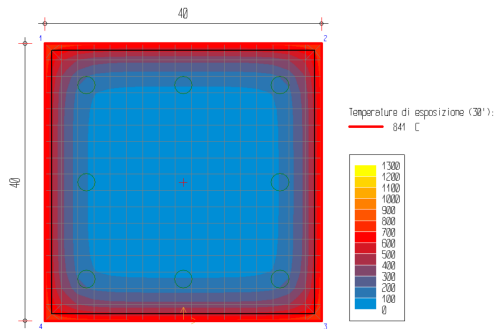


Figure 3.2: Heat distribution at 30 minutes

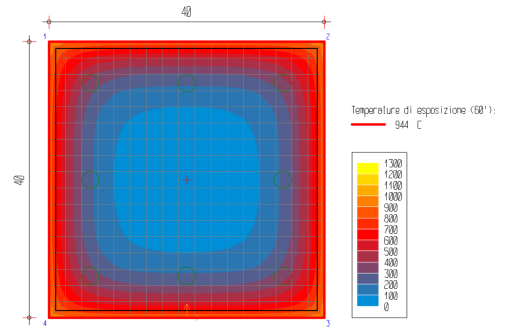


Figure 3.3: Heat distribution at 60 minutes

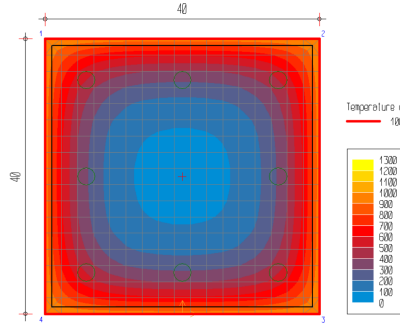


Figure 3.4: Heat distribution at 90 minutes

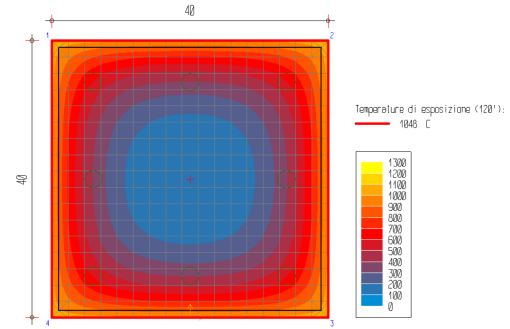


Figure 3.5: Heat distribution at 120 minutes

3.2 Mechanical Response

Once the results of the thermal response are obtained, it is possible to calculate the mechanical response of the section. This has been done with Python, and the different parts of the code will be shown and explained throughout this chapter.

3.2.1 Basics of the Model

First of all, the geometrical and thermal data from the thermal model needs to be exported as a table. The geometrical data needed for each finite element are: area (considered in mm^2 in this study) and position (z and y coordinate, also in mm). Aside from this, the remaining information necessary is the temperature (in $^{\circ}\text{C}$) and the material ("C" for concrete, "S" for structural steel, and "R" for reinforcing steel).

The approach considered for the estimation of the interaction domain consists of a 5-point approach, where each point represents a meaningful part of the behavior of the columns. The points are:

- P_1) Point with highest positive axial load. The whole section is tensed and there is no moment (all the stresses in the section are associated with tension).
- P_2) Point with highest negative axial load. The whole section is under compression and once again there is no moment present (all the stresses in the section are associated with compression).

- P_3) Point with zero axial load. The section is deformed under the effect of moment, but the compressive and tensile forces are equal to each other, resulting in a net axial force of zero.
- P_4) Moment is equal to that of P_3 , but the axial load is different from zero. This is a point in the descending branch of the interaction domain, when the axial compressive load is past the value that allows for the highest moment.
- P_5) This is the point where the moment in the section is at its peak. For this, a compressive axial load between that found in P_4 and P_3 (zero) is present.

This 5-point approach can be seen more clearly in figure 3.6, where each point is visible and the interaction domain is computed. The hatched area constitutes the area where (N,M) pairs are below the limit strength of the cross-section, and as such the section would be verified for those solicitations.

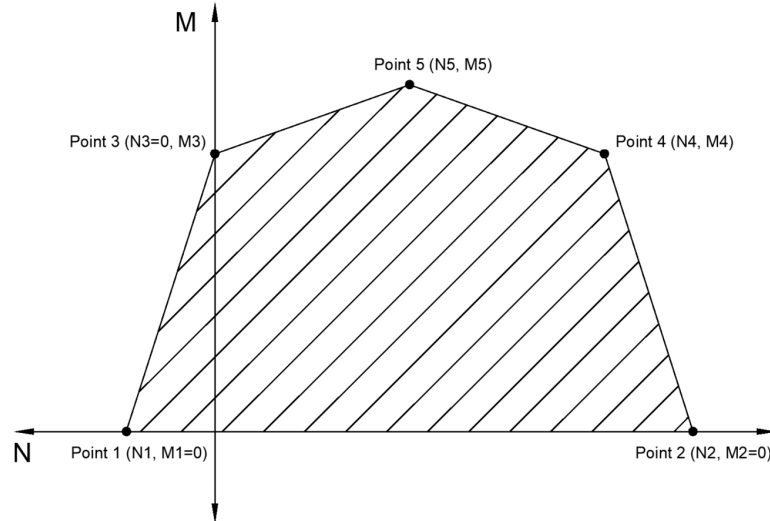


Figure 3.6: 5-Point approach

To find these points, we need to use formulas 3.2 to 3.4 [34] in order to verify the equilibrium conditions inside the cross-section.

$$N = \int_A \sigma_x dA \quad (3.2)$$

$$M_z = \int_A y \sigma_x dA \quad (3.3)$$

$$M_y = \int_A z \sigma_x dA \quad (3.4)$$

However, given that we are dealing with finite elements, these equations can be rewritten as equations 3.5, 3.6, and 3.7 without the need for integrals in order to make evaluation easier. In these, i refers to a finite element while n is the total amount of finite elements.

$$N = \sum_{i=1}^n \sigma_{x,i} \cdot A_i \quad (3.5)$$

$$M_z = \sum_{i=1}^n y_i \cdot \sigma_{x,i} \cdot A_i \quad (3.6)$$

$$M_y = \sum_{i=1}^n z_i \cdot \sigma_{x,i} \cdot A_i \quad (3.7)$$

Through these equations, and knowing the distribution of temperature in the section, it is possible to calculate the contribution of each finite element in the mesh to each of these internal actions. As can be seen in figures 3.7 and 3.8, it is possible to obtain the average temperature within each finite element from the thermal response through the program used.

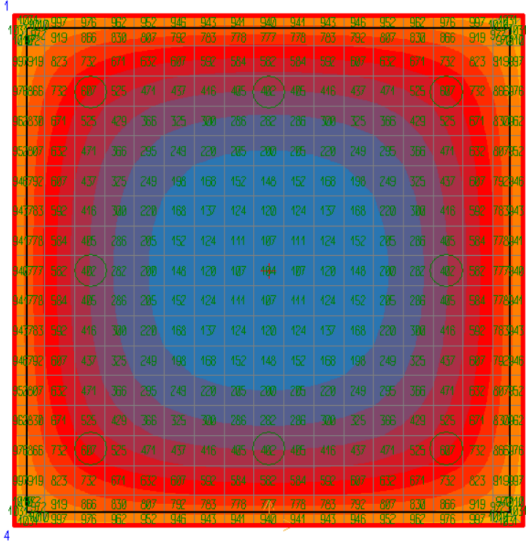


Figure 3.7: Temperature expected on concrete and structural steel elements at 120 minutes

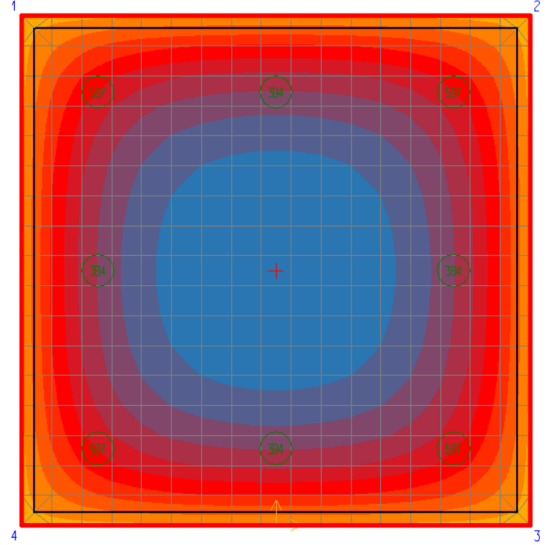


Figure 3.8: Temperature expected on reinforcing bars at 120 minutes

In order to find the strain at each of the finite elements, a function was defined for this. It can be seen in the following code:

```

1 def deformation(ec, es, h, y):
2     if ec==0.2:
3         e=0.2
4     elif ec==0:
5         e=es*(h-y)/h
6     elif es>0:
7         c=(-ec*h)/(-ec+es)
8         if y<=(h-c):
9             e=(es*(h-c-y))/(h-c)
10        else:
11            e=(ec*(y-(h-c)))/c
12    elif es<=0:
13        e=es+(ec-es)*y/h
14    return e

```

In this function, ec represents the strain at the highest point of the section while es is the strain at the bottom of it. This function takes advantage of the linear distribution of stresses to find the strain of an arbitrary finite element positioned at y (or z) in a section of height h (or width b).

3.2.2 Stress-Strain Relationships

In order to evaluate the longitudinal tension state within each finite element, which is needed for the evaluation of equations 3.5 to 3.7, we need to define the stress-strain relationships to be used for each material.

Concrete

Eurocode 2, part 1-2 [35] provides a stress-strain relationship to be considered for concrete at higher temperatures. This can be modeled as seen in equation 3.8 until the peak. The second phase can be considered by any descending linear and non-linear models arriving at $\epsilon_{cu1,\theta}$. This behavior can also be seen in figure 3.9. For what concerns this study, a linear descending branch arriving at a stress of 0 was considered.

$$\sigma_c = \frac{3\epsilon f_{c,\theta}}{\epsilon_{c1,\theta} \left(2 + \left(\frac{\epsilon}{\epsilon_{c1,\theta}}\right)^3\right)} \text{ for } \epsilon \leq \epsilon_{c1,\theta} \quad (3.8)$$

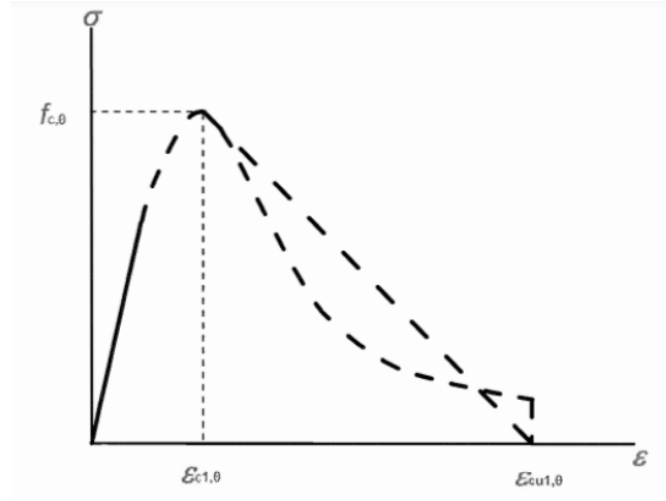


Figure 3.9: Stress-Strain relationship of concrete at higher temperature, in accordance to Eurocode 2 part 1-2 [35]

Concrete temp. θ [°C]	Siliceous aggregates			Calcareous aggregates		
	$f_{c,\theta} / f_{ck}$ [-]	$\varepsilon_{c1,\theta}$ [-]	$\varepsilon_{cu1,\theta}$ [-]	$f_{c,\theta} / f_{ck}$ [-]	$\varepsilon_{c1,\theta}$ [-]	$\varepsilon_{cu1,\theta}$ [-]
1	2	3	4	5	6	7
20	1,00	0,0025	0,0200	1,00	0,0025	0,0200
100	1,00	0,0040	0,0225	1,00	0,0040	0,0225
200	0,95	0,0055	0,0250	0,97	0,0055	0,0250
300	0,85	0,0070	0,0275	0,91	0,0070	0,0275
400	0,75	0,0100	0,0300	0,85	0,0100	0,0300
500	0,60	0,0150	0,0325	0,74	0,0150	0,0325
600	0,45	0,0250	0,0350	0,60	0,0250	0,0350
700	0,30	0,0250	0,0375	0,43	0,0250	0,0375
800	0,15	0,0250	0,0400	0,27	0,0250	0,0400
900	0,08	0,0250	0,0425	0,15	0,0250	0,0425
1000	0,04	0,0250	0,0450	0,06	0,0250	0,0450
1100	0,01	0,0250	0,0475	0,02	0,0250	0,0475
1200	0,00	-	-	0,00	-	-

Figure 3.10: Relevant deformation values and resistance ratios for concrete, in accordance to [35]

As for the different parameters observed in figure 3.10, we can observe that the peak compressive strength decreases with temperature as the deformation limits

become larger (and so the ductility increases). For instance, it is possible to note that concrete at 600 °C has a peak compressive strength of about 45% of its peak compressive strength at room temperature, but the deformation required to achieve this peak is 10x larger. For this same temperature, we can also note that the ultimate deformation $\epsilon_{cu1,\theta}$ increases by around 75%.

This stress-strain relationship for concrete was defined as a function in python in the following way:

```

1 def SSRelC (k,eps1,epsu1,eps):
2     if eps>0:
3         s=0
4     else:
5         if abs(eps)<=eps1:
6             s=-((3*abs(eps)*30*k)/(eps1*(2+(abs(eps)/eps1)**3)))
7         elif abs(eps)<=(epsu1+0.00001):
8             s=-((30*k)/(epsu1-eps1)*eps1+30*k*(30*k)/
9                 (epsu1-eps1)*abs(eps))
10        else:
11            s=0 #Concrete is cracked
12    return s

```

As can be seen in the code, the $f_{c,k}$ value considered was 30 MPa as the concrete treated throughout this study belongs to the C30/37 class.

While the parameter needed for running this function (those provided by the table in figure 3.10) were obtained from the following function, which only depends on concrete temperature:

```

1 def ParC (t):
2     if t<=100:
3         k=1
4         eps1= 0.0025+((t-20)/(100-20))*(0.004-0.0025)
5         epsu1= 0.02+((t-20)/(100-20))*(0.0225-0.02)
6     elif t<=200:
7         k=1+((t-100)/(100))*(0.95-1)
8         eps1= 0.004+((t-100)/(100))*(0.0055-0.004)
9         epsu1= 0.0225+((t-100)/(100))*(0.0250-0.0225)
10    elif t<=300:
11        k=0.95+((t-200)/(100))*(0.85-0.95)
12        eps1= 0.0055+((t-200)/(100))*(0.0070-0.0055)
13        epsu1= 0.0250+((t-200)/(100))*(0.0275-0.0250)
14    elif t<=400:

```

```

15     k=0.85+((t-300)/(100))*(0.75-0.85)
16     eps1= 0.0070+((t-300)/(100))*(0.01-0.0070)
17     epsu1= 0.0275+((t-300)/(100))*(0.03-0.0275)
18     elif t<=500:
19         k=0.75+((t-400)/(100))*(0.6-0.75)
20         eps1= 0.01+((t-400)/(100))*(0.015-0.01)
21         epsu1= 0.03+((t-400)/(100))*(0.0325-0.03)
22     elif t<=600:
23         k=0.6+((t-500)/(100))*(0.45-0.6)
24         eps1= 0.015+((t-500)/(100))*(0.025-0.015)
25         epsu1= 0.0325+((t-500)/(100))*(0.035-0.0325)
26     elif t<=700:
27         k=0.45+((t-600)/(100))*(0.3-0.45)
28         eps1= 0.025
29         epsu1= 0.035+((t-600)/(100))*(0.0375-0.035)
30     elif t<=800:
31         k=0.3+((t-700)/(100))*(0.15-0.3)
32         eps1= 0.025
33         epsu1= 0.0375+((t-700)/(100))*(0.04-0.0375)
34     elif t<=900:
35         k=0.15+((t-800)/(100))*(0.08-0.15)
36         eps1= 0.025
37         epsu1= 0.04+((t-800)/(100))*(0.0425-0.04)
38     elif t<=1000:
39         k=0.08+((t-900)/(100))*(0.04-0.08)
40         eps1= 0.025
41         epsu1= 0.0425+((t-900)/(100))*(0.045-0.0425)
42     elif t<=1100:
43         k=0.04+((t-1000)/(100))*(0.01-0.04)
44         eps1= 0.025
45         epsu1= 0.045+((t-1000)/(100))*(0.0475-0.045)
46     elif t<=1200:
47         k=0.01+((t-1100)/(100))*(0-0.01)
48         eps1= 0.025
49         epsu1= 0.0475
50     else:
51         k="F"
52         eps1="F"
53         epsu1="F"
54
55     return [k, eps1, epsu1]

```

It is important to note that, regarding this study, only siliceous aggregate concrete was considered and as such only the first half of the table in figure 3.10 was

coded.

For didactic purposes, also a regular parabola rectangle relation (as contemplated in Eurocode 2 for non-fire design [3]) was considered for the stress-strain relationship of concrete in order to compare the results obtained through both relationships. In order to account for the temperature in the section, this function was scaled by the factors obtained from the table in figure 3.10. The resulting relationship can be seen in the following code.

```

1 def SSRELCPROVA (k,eps1,epsu1,eps):
2     if eps>0:
3         s=0
4     else:
5         if abs(eps)<=eps1:
6             s=-(30*k)*(1-(1-abs(eps)/eps1)**2)
7         elif abs(eps)<=(epsu1+0.00001):
8             s=-30*k
9         else:
10            s=0 #Concrete is cracked
11     return s

```

Examples of both these stress-strain relationships for concrete at a temperature of 357 °C are shown in figures 3.11 and 3.12.

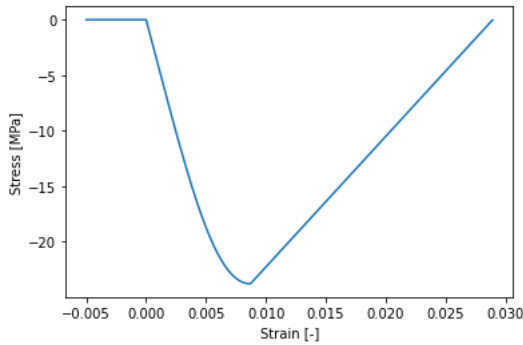


Figure 3.11: Stress-strain relationship modeled by SSRELC

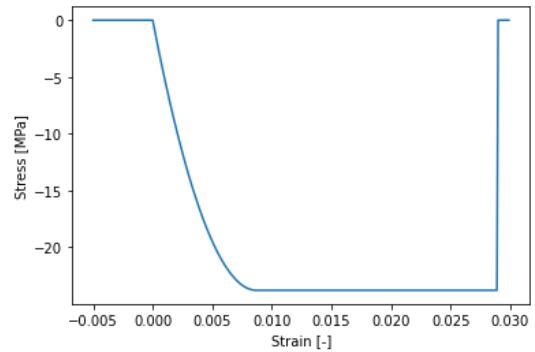


Figure 3.12: Stress-strain relationship modeled by SSRELCPROVA

It can be noted that these stress-strain relationships produce negative stresses as only compressive stresses can be bore by concrete. Aside from this, they were plotted for positive values of deformation for representation reasons, but the functions only provide stress if the strain is negative (compression).

It is also important to mention that, besides the fact that the compressive strength decreases as temperature increases, there are some parameters that result in a "positive" increment of strength in a fire scenario. For instance, the safety factors α_{cc} (usually taken as 0.85) and γ_c (usually taken as 1.5) are both 1 under fire scenario, and as such don't reduce the compressive strength of concrete. This usually may result in an increased resistance (relative to room temperature) at the lowest temperatures considered for the fire scenario.

Structural and Reinforcing Steel

The relationship presented for reinforcing steel in EC2 part 1-2 [35] and structural steel in EC3 part 1-2 [36] show the same behavior, and as such will only be shown here once. This follows the same logic as the one previously shown for concrete and can be fully described through figures 3.13, 3.14, and 3.15.

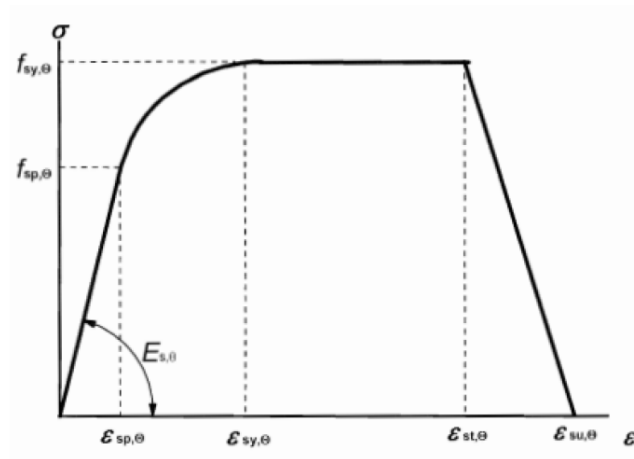


Figure 3.13: Stress-Strain relationship for steel at higher temperature, in accordance to [36]

Range	Stress $\sigma(\theta)$	Tangent modulus
$\varepsilon_{sp,\theta}$	$\varepsilon E_{s,\theta}$	$E_{s,\theta}$
$\varepsilon_{sp,\theta} \leq \varepsilon \leq \varepsilon_{sy,\theta}$	$f_{sp,\theta} - c + (b/a)[a^2 - (\varepsilon_{sy,\theta} - \varepsilon)^2]^{0,5}$	$\frac{b(\varepsilon_{sy,\theta} - \varepsilon)}{a[a^2 - (\varepsilon - \varepsilon_{sy,\theta})^2]^{0,5}}$
$\varepsilon_{sy,\theta} \leq \varepsilon \leq \varepsilon_{st,\theta}$	$f_{sy,\theta}$	0
$\varepsilon_{st,\theta} \leq \varepsilon \leq \varepsilon_{su,\theta}$	$f_{sy,\theta} [1 - (\varepsilon - \varepsilon_{st,\theta}) / (\varepsilon_{su,\theta} - \varepsilon_{st,\theta})]$	-
$\varepsilon = \varepsilon_{su,\theta}$	0,00	-
Parameter *)	$\varepsilon_{sp,\theta} = f_{sp,\theta} / E_{s,\theta}$ $\varepsilon_{sy,\theta} = 0,02$ $\varepsilon_{st,\theta} = 0,15$ $\varepsilon_{su,\theta} = 0,20$ Class A reinforcement: $\varepsilon_{st,\theta} = 0,05$ $\varepsilon_{su,\theta} = 0,10$	
Functions	$a^2 = (\varepsilon_{sy,\theta} - \varepsilon_{sp,\theta})(\varepsilon_{sy,\theta} - \varepsilon_{sp,\theta} + c/E_{s,\theta})$ $b^2 = c (\varepsilon_{sy,\theta} - \varepsilon_{sp,\theta}) E_{s,\theta} + c^2$ $c = \frac{(f_{sy,\theta} - f_{sp,\theta})^2}{(\varepsilon_{sy,\theta} - \varepsilon_{sp,\theta}) E_{s,\theta} - 2(f_{sy,\theta} - f_{sp,\theta})}$	

Figure 3.14: Definition of stress-Strain relationship for steel at higher temperature, in accordance to [36]

Steel Temperature θ [°C]	$f_{sy,\theta} / f_{yk}$		$f_{sp,\theta} / f_{yk}$		$E_{s,\theta} / E_s$	
	hot rolled	cold worked	hot rolled	cold worked	hot rolled	cold worked
1	2	3	4	5	6	7
20	1,00	1,00	1,00	1,00	1,00	1,00
100	1,00	1,00	1,00	0,96	1,00	1,00
200	1,00	1,00	0,81	0,92	0,90	0,87
300	1,00	1,00	0,61	0,81	0,80	0,72
400	1,00	0,94	0,42	0,63	0,70	0,56
500	0,78	0,67	0,36	0,44	0,60	0,40
600	0,47	0,40	0,18	0,26	0,31	0,24
700	0,23	0,12	0,07	0,08	0,13	0,08
800	0,11	0,11	0,05	0,06	0,09	0,06
900	0,06	0,08	0,04	0,05	0,07	0,05
1000	0,04	0,05	0,02	0,03	0,04	0,03
1100	0,02	0,03	0,01	0,02	0,02	0,02
1200	0,00	0,00	0,00	0,00	0,00	0,00

Figure 3.15: Relevant ratios for steel at higher temperatures, in accordance to [36]

The stress-strain relationship was also coded in a similar fashion to the relationships for concrete, where the function SSRelS was defined as follows.

```

1 def SSRelS (ksy, ksp, kE, eps, C):
2     if C=="R":
3         fy=450 #MPa
4         E = 200000 #MPa
5     elif C=="S":
6         fy=355 #MPa
7         E = 210000 #MPa
8     ##Important Parameters and Values
9     fsy=ksy*fy
10    fsp=ksp*fy
11    Eth=kE*E
12    eps_sp=fsp/Eth
13    eps_sy=0.02
14    eps_st=0.15
15    eps_su=0.2
16    ##Functions
17    c=(fsy-fsp)**2/((eps_sy-eps_sp)*Eth-2*(fsy-fsp))
18    b2=c*(eps_sy-eps_sp)*Eth+c**2
19    a2=(eps_sy-eps_sp)*(eps_sy-eps_sp+c/Eth)
20    ##Relation
21    if abs(eps)<=eps_sp:
22        if eps>=0:
23            s=abs(eps)*Eth
24        else:
25            s=-abs(eps)*Eth
26    elif abs(eps)<=eps_sy:
27        if eps>=0:
28            s=fsp-c+(b2**(0.5)/a2**(0.5))
29            *(a2-(eps_sy-abs(eps))**2)**0.5
30        else:
31            s=-(fsp-c+(b2**(0.5)/a2**(0.5))
32            *(a2-(eps_sy-abs(eps))**2)**0.5)
33    elif abs(eps)<=eps_st:
34        if eps>=0:
35            s=fsy
36        else:
37            s=-fsy
38    elif abs(eps)<=(eps_su+0.00001):
39        if eps>=0:
40            s=fsy*(1-(abs(eps)-eps_st)/(eps_su-eps_st))
41        else:

```

```

42         s=-(fsy*(1-(abs(eps)-eps_st)/(eps_su-eps_st)))
43     else:
44         s=0
45     return s

```

As can be seen from the code, in this case, the steel class both for the structural profile and the reinforcing bars was considered in the stress-strain relationship. This is, a yielding stress $f_y = 355$ MPa was considered for structural steel S355 and $f_y = 450$ MPa for reinforcing bars B450C.

Analog to the case for concrete, the function ParS was defined in order to obtain the parameters required for the evaluation of the stress-strain relationship. This makes use of the values found in the table in figure 3.15, taking into consideration only the values associated with hot-rolled steel (as is the case worked in this study). This code can be seen below.

```

1  def ParS (t):
2      if t<=100:
3          ksy=1
4          ksp= 1
5          kE= 1
6      elif t<=200:
7          ksy=1
8          ksp=1+((t-100)/(100))*(0.81-1)
9          kE=1+((t-100)/(100))*(0.9-1)
10     elif t<=300:
11         ksy=1
12         ksp=0.81+((t-200)/(100))*(0.61-0.81)
13         kE=0.9+((t-200)/(100))*(0.8-0.9)
14     elif t<=400:
15         ksy=1
16         ksp=0.61+((t-300)/(100))*(0.42-0.61)
17         kE=0.8+((t-300)/(100))*(0.7-0.8)
18     elif t<=500:
19         ksy=1+((t-400)/(100))*(0.78-1)
20         ksp= 0.42+((t-400)/(100))*(0.36-0.42)
21         kE= 0.7+((t-400)/(100))*(0.6-0.7)
22     elif t<=600:
23         ksy=0.78+((t-500)/(100))*(0.47-0.78)
24         ksp= 0.36+((t-500)/(100))*(0.18-0.36)
25         kE= 0.6+((t-500)/(100))*(0.31-0.6)
26     elif t<=700:
27         ksy=0.47+((t-600)/(100))*(0.23-0.47)

```

```

28     ksp= 0.18+((t-600)/(100))*(0.07-0.18)
29     kE= 0.31+((t-600)/(100))*(0.13-0.31)
30     elif t<=800:
31         ksy=0.23+((t-700)/(100))*(0.11-0.23)
32         ksp= 0.07+((t-700)/(100))*(0.05-0.07)
33         kE= 0.13+((t-700)/(100))*(0.09-0.13)
34     elif t<=900:
35         ksy=0.11+((t-800)/(100))*(0.06-0.11)
36         ksp= 0.05+((t-800)/(100))*(0.04-0.05)
37         kE= 0.09+((t-800)/(100))*(0.07-0.09)
38     elif t<=1000:
39         ksy=0.06+((t-900)/(100))*(0.04-0.06)
40         ksp= 0.04+((t-900)/(100))*(0.02-0.04)
41         kE= 0.07+((t-900)/(100))*(0.04-0.07)
42     elif t<=1100:
43         ksy=0.04+((t-1000)/(100))*(0.02-0.04)
44         ksp=0.02+((t-1000)/(100))*(0.01-0.02)
45         kE= 0.04+((t-1000)/(100))*(0.02-0.04)
46     elif t<=1200:
47         ksy=0.02+((t-1100)/(100))*(0-0.02)
48         ksp=0.01+((t-1100)/(100))*(0-0.01)
49         kE= 0.02+((t-1100)/(100))*(0-0.02)
50     else:
51         ksy="F"
52         ksp="F"
53         kE="F"
54
55     return [ksy, ksp, kE]

```

An example of what this stress-strain relationship looks like for reinforcing steel B450C at a temperature of 897 °C looks like can be appreciated in figure 3.16.

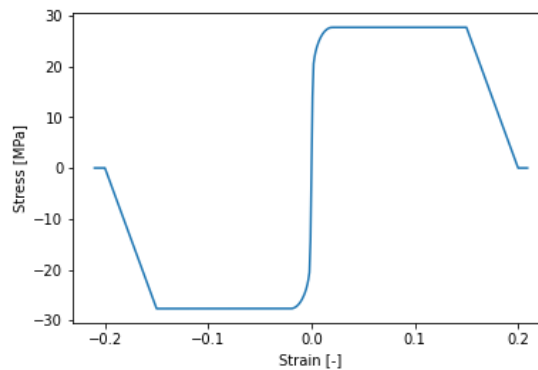


Figure 3.16: Stress-strain relationship coded for steel

3.2.3 Calculation of 5 Point Approach

Point 1 - Full Tension

This point refers to when the entire section is under the same positive strain. In this case, given that the plastic range for steel is constant regardless of the temperature, the deformation could just be set at any value between 0.02 and 0.15. Nonetheless, a more general approach was taken where the entire stress ranges from 0 to $\epsilon_{su,\theta} = 0.2$, and the maximum value of axial load is recorded. The code used to obtain this result can be visualized below.

```

1 det=[]
2 esT=0
3 while esT<=0.2:
4     L=[esT,esT]
5     det.append(L)
6     esT+=0.001
7
8 Nt=[0]*len(det)
9 Mt=[0]*len(det)
10
11 k=0
12 while k <len(data1):
13     y=data1.loc[k].at["Y"]
14     z=b/2+data1.loc[k].at["Z"]
15     mat=data1.loc[k].at["Type"]
16     theta=data1.loc[k].at["Temp"]
17     A=data1.loc[k].at["Area"]
18     rz=abs(h/2-y)
19     ry=abs(b/2-z)
20     j=0
21     while j<len(det):
22         e=det[j][0]
23         if mat=="C":
24             [kc, eps1, epsu1]=ParC(theta)
25             if SSC==1:
26                 ss=SSRelC (kc, eps1, epsu1 ,e)
27             elif SSC==2:
28                 ss=SSRelCPROVA (kc, eps1, epsu1 ,e)
29         else:
30             [ksy, ksp, kE]=ParS(theta)
31             ss=SSRelS (ksy, ksp, kE, e, mat)
32         n=A*ss
33         Nt[j]=Nt[j]+n

```

```

34         if Mdir=="z":
35             if y<(h/2):
36                 m=n*rz
37             else:
38                 m=-n*rz
39         elif Mdir=="y":
40             if z<(b/2):
41                 m=n*ry
42             else:
43                 m=-n*ry
44         Mt[j]=Mt[j]+m
45         j+=1
46     k+=1
47
48 Nt[:]=[x / 1000 for x in Nt] #Conversion to kN
49 Mt[:]=[x / 1000000 for x in Mt] #Conversion to kNm
50
51 indext=0
52 peakNt=0
53 ft=0
54 while ft<len(Nt):
55     if Nt[ft]>peakNt:
56         indext=ft
57         peakNt=Nt[ft]
58     ft+=1

```

There are a few things worth noting in this code (and also the ones present for the next points):

- The variable "data1" contains information regarding the mesh and heat distribution within the section. This is the variable where all the geometrical data, temperature, and material of each finite element are stored.
- The variable "SSC" represents the type of stress-strain relationship of concrete used for the analysis. This value is 1 if the first relationship is used, and 2 if the modified parabola-rectangle is taken into account. In this particular case, the SS relationship taken for concrete is not relevant as the whole section is under tension, but it is relevant for the remaining 4 points.
- In this particular case, the specific M_t value associated with the peak axial load value is disregarded as 0 instead of calculated, but this is due to the symmetry of geometry and fire exposure in the section.

Point 2 - Full Compression

This point is associated with when the cross-section is under full compression. Analog to point 1, due to the geometrical symmetry of the section and the symmetry in fire exposure, a flat state of stress means that the bending moment in the section is 0.

In this case, it is necessary to consider a wide array of flat deformation profiles as it is impossible to know beforehand what profile will yield the highest compressive strength. As the temperature of each concrete finite element varies, it becomes impossible to define a deformation value for the peak concrete compressive strength of the section given that said deformation value is different for all concrete finite elements. With this in mind, it is possible to define many flat deformation profiles, from 0 to -0.2 (value which is higher than the maximum possible $\epsilon_{cu1,\theta}$ for concrete) and evaluate the axial load (using equation 3.5) for each of them. In this way, it is possible to find the highest axial compressive load and the deformation profile which induces it. This is all taken into account thoroughly in the following code.

```

1  dec=[]
2  esC=0
3  while esC>=-0.2:
4      L=[esC,esC]
5      dec.append(L)
6      esC-=0.001
7
8  Nc=[0]*len(dec)
9  Mc=[0]*len(dec)
10
11 k=0
12 while k <len(data1):
13     y=data1.loc[k].at["Y"]
14     z=b/2+data1.loc[k].at["Z"]
15     mat=data1.loc[k].at["Type"]
16     theta=data1.loc[k].at["Temp"]
17     A=data1.loc[k].at["Area"]
18     rz=abs(h/2-y)
19     ry=abs(b/2-z)
20     j=0
21     while j<len(dec):
22         e=dec[j][0]
23         if mat=="C":
24             [kc, eps1, epsu1]=ParC(theta)
25             if SSC==1:
```

```

26         ss=SSRelC (kc, eps1, epsu1 ,e)
27     elif SSC==2:
28         ss=SSRelCPROVA (kc, eps1, epsu1 ,e)
29     else:
30         [ksy, ksp, kE]=ParS(theta)
31         ss=SSRelS (ksy, ksp, kE, e, mat)
32     n=A*ss
33     Nc[j]=Nc[j]+n
34
35     if Mdir=="z":
36         if y<(h/2):
37             m=n*rz
38         else:
39             m=-n*rz
40     elif Mdir=="y":
41         if z<(b/2):
42             m=n*ry
43         else:
44             m=-n*ry
45     Mc[j]=Mc[j]+m
46     j+=1
47     k+=1
48
49 Nc[:]=[x / 1000 for x in Nc] #Conversion to kN
50 Mc[:]=[x / 1000000 for x in Mc] #Conversion to kNm
51
52 index=0
53 peakNc=0
54 f=0
55 while f<len(Nc):
56     if Nc[f]<peakNc:
57         index=f
58         peakNc=Nc[f]
59     f+=1

```

Point 3 - Axial Load = 0, $M \neq 0$

This point was obtained by setting the deformation at the bottom of the section at the yielding deformation $\epsilon_{sy,\theta} = 0.02$, and varying the deformation at the top of the section in order to find the deformation profile that returns an axial load of 0 (or the closest value to it, given that discretized variations in deformation are being used and it is impossible to guarantee the exact result). This was done through the following code.


```

1 dem=[]
2 esM=0.02
3 ec=0
4 while ec<=0.03:
5     L=[esM,-ec]
6     dem.append(L)
7     ec+=0.0001
8
9 Nm=[0]*len(dem)
10 Mm=[0]*len(dem)
11
12 k=0
13 while k <len(data1):
14     y=data1.loc[k].at["Y"]
15     z=b/2+data1.loc[k].at["Z"]
16     mat=data1.loc[k].at["Type"]
17     theta=data1.loc[k].at["Temp"]
18     A=data1.loc[k].at["Area"]
19     rz=abs(h/2-y)
20     ry=abs(b/2-z)
21     j=0
22     while j<len(dem):
23         if Mdir=="z":
24             e=deformation(dem[j][1], dem[j][0], h, y)
25         elif Mdir=="y":
26             e=deformation(dem[j][1], dem[j][0], b, z)
27         if mat=="C":
28             [kc, eps1, epsu1]=ParC(theta)
29             if SSC==1:
30                 ss=SSRelC (kc,abs(eps1),abs(epsu1),e)
31             elif SSC==2:
32                 ss=SSRelCPROVA (kc,abs(eps1),abs(epsu1),e)
33
34         else:
35             [ksy, ksp, kE]=ParS(theta)
36             ss=SSRelS (ksy, ksp, kE, e, mat)
37
38         n=A*ss
39         Nm[j]=Nm[j]+n
40
41         if Mdir=="z":
42             if y<(h/2):
43                 m=n*rz
44             else:

```

```

45         m=-n*rz
46     elif Mdir=="y":
47         if z<(b/2):
48             m=n*ry
49         else:
50             m=-n*ry
51         Mm[j]=Mm[j]+m
52         j+=1
53     k+=1
54
55 Nm[:]=[x / 1000 for x in Nm] #Conversion to kN
56 Mm[:]=[x / 1000000 for x in Mm] #Conversion to kNm
57
58 indexm=0
59 peakMm=0
60 difm=1000
61 fm=0
62 while fm<len(Nm):
63     dif=abs(Nm[fm])
64     if dif<difm:
65         difm=dif
66         indexm=fm
67         peakMm=Mm[fm]
68     fm+=1

```

The decision to set the bottom deformation at the yielding value $\epsilon_{sy,\theta} = 0.02$ instead of the ultimate plastic deformation value $\epsilon_{st,\theta} = 0.15$ came from an iterative process. In this, it was found that, despite the former ($\epsilon_{sy,\theta}$) providing a smaller contribution to the moment from the steel (as less steel is in yielding) it allowed for a greater contribution from concrete that compensated the situation.

Point 4 - Axial Load $\neq 0$, $M = M_{P_3}$

When analyzing the interaction domain of a regular reinforced concrete column, we can observe that the top of the domain (above points 3 and 4, in this study) behaves as would the unreinforced concrete section [37]. This behavior can be seen more clearly in Figure 3.17.

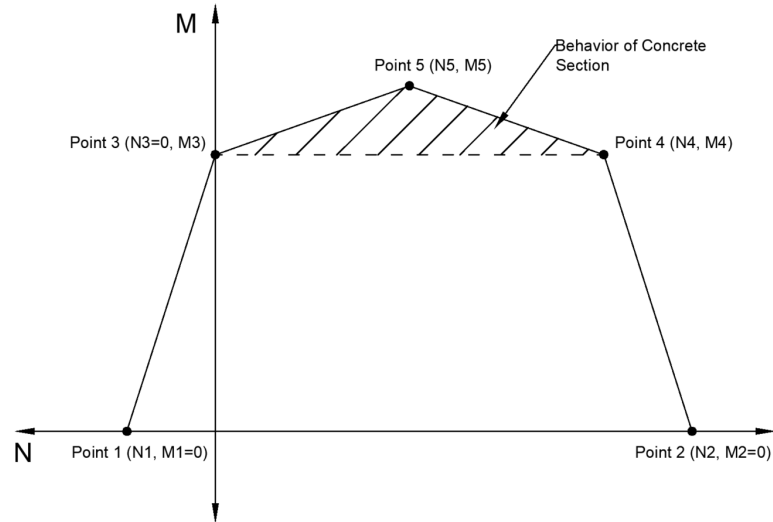


Figure 3.17: Behavior of concrete section

This kind of behavior can then be extrapolated to the composite case as the base physical concepts remain the same. With this under consideration, it is possible to estimate the axial load for point 4 as the maximum possible compression load supported only by the plain concrete of the section. In this way, the same approach used for the calculation of the axial load for the second point was taken, but only considering the contribution of concrete. The code employed for this purpose can be found below.

```

1 ded=[]
2 esD=0
3 while esD>=-0.2:
4     L=[esD,esD]
5     ded.append(L)
6     esD-=0.001
7
8 Nd=[0]*len(ded)
9 Md=[0]*len(ded)
10
11 k=0
12 while k <len(data1):
13     y=data1.loc[k].at["Y"]
14     z=b/2+data1.loc[k].at["Z"]
15     mat=data1.loc[k].at["Type"]
16     theta=data1.loc[k].at["Temp"]
17     A=data1.loc[k].at["Area"]

```

```

18     rz=abs(h/2-y)
19     ry=abs(b/2-z)
20     j=0
21     while j<len(ded):
22         e=ded[j][0]
23         if mat=="C":
24             [kc, eps1, epsu1]=ParC(theta)
25             if SSC==1:
26                 ss=SSRelC (kc, eps1, epsu1 ,e)
27             elif SSC==2:
28                 ss=SSRelCPROVA (kc, eps1, epsu1 ,e)
29         else:
30             ss=0
31         n=A*ss
32         Nd[j]=Nd[j]+n
33
34         if Mdir=="z":
35             if y<(h/2):
36                 m=n*rz
37             else:
38                 m=-n*rz
39         elif Mdir=="y":
40             if z<(b/2):
41                 m=n*ry
42             else:
43                 m=-n*ry
44         Md[j]=Md[j]+m
45         j+=1
46     k+=1
47
48 Nd[:]=[x / 1000 for x in Nd] #Conversion to kN
49 Md[:]=[x / 1000000 for x in Md] #Conversion to kNm
50
51 indexd=0
52 peakNd=0
53 fd=0
54 while fd<len(Nd):
55     if Nd[fd]<peakNd:
56         indexd=fd
57         peakNd=Nd[fd]
58     fd+=1

```

Point 5 - Axial Load $\neq 0$, $M = M_{max}$

The 5th point is not easily defined due to the variation in the deformation limits of the stress-strain relationship of concrete through the cross-section. With this in mind, an approximative approach was taken and the neutral axis was fixed in the middle of the cross-section. Through this approach, the deformation at the top of the section is equal in absolute value but different in sign to that at the bottom of the section. The extreme deformation values are then varied from 0 to 0.2 (or -0.2 as in the case of the top fibers). In this way, the moment and axial load for each deformation profile are computed, and the pair with the maximum moment corresponds to point 5. The following code was used for the calculation of this point.

```

1 de5=[]
2 es5=0
3 while es5<=0.2:
4     L=[es5,-es5]
5     de5.append(L)
6     es5+=0.001
7
8 N5=[0]*len(de5)
9 M5=[0]*len(de5)
10
11 k=0
12 while k <len(data1):
13     y=data1.loc[k].at["Y"]
14     z=b/2+data1.loc[k].at["Z"]
15     mat=data1.loc[k].at["Type"]
16     theta=data1.loc[k].at["Temp"]
17     A=data1.loc[k].at["Area"]
18     rz=abs(h/2-y)
19     ry=abs(b/2-z)
20     j=0
21     while j<len(de5):
22         if Mdir=="z":
23             e=deformation(de5[j][1], de5[j][0], h, y)
24         elif Mdir=="y":
25             e=deformation(de5[j][1], de5[j][0], b, z)
26         if mat=="C":
27             [kc, eps1, epsu1]=ParC(theta)
28             if SSC==1:
29                 ss=SSRelC (kc, eps1, epsu1 ,e)
30             elif SSC==2:
31                 ss=SSRelCPROVA (kc, eps1, epsu1 ,e)

```

```

32     else:
33         [ksy, ksp, kE]=ParS(theta)
34         ss=SSRelS (ksy, ksp, kE, e, mat)
35         n=A*ss
36         N5[j]=N5[j]+n
37
38         if Mdir=="z":
39             if y<(h/2):
40                 m=n*rz
41             else:
42                 m=-n*rz
43         elif Mdir=="y":
44             if z<(b/2):
45                 m=n*ry
46             else:
47                 m=-n*ry
48         M5[j]=M5[j]+m
49         j+=1
50     k+=1
51
52     N5[:]=[x / 1000 for x in N5] #Conversion to kN
53     M5[:]=[x / 1000000 for x in M5] #Conversion to kNm
54
55     index5=0
56     peakM5=0
57     peakN5=0
58     f5=0
59     while f5<len(M5):
60         if M5[f5]>peakM5:
61             index5=f5
62             peakM5=M5[f5]
63             peakN5=N5[f5]
64         f5+=1

```

3.3 Results

This method was applied to the same column as mentioned previously, with overall dimensions of 40x40 cm, a structural steel thickness of 10 mm, and 8 $\phi 26$ reinforcing bars distributed symmetrically through the section with a concrete cover of 5 cm (section also visible in figure 3.1). The resistance for this column after 2 hours of exposure to fire can be observed in figure 3.18. In this, the gray curve describes the interaction domain considering the mechanical tool developed during this study and the stress-strain relationship for concrete as described by function SSRelC, while the orange curve considers the same approach but with the modified parabola-rectangle SS relationship. Also, the blue curve, considered for reference, is the result obtained through the mechanical analysis tool of the IS.FUOCO module.

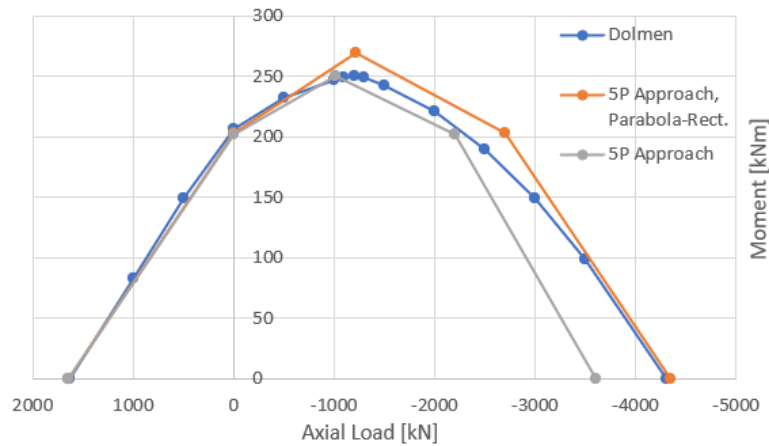


Figure 3.18: Results for P40x40t10 after 120 minutes

The same analysis was also realized extensively to the two columns described in figure 4.9. The results for column P40x80t10 can be observed from figure 3.19 to 3.26, with figures 3.19-3.22 representing the behavior in the main axis (z) and 3.23-3.26 describing the behavior of the weak axis (y).

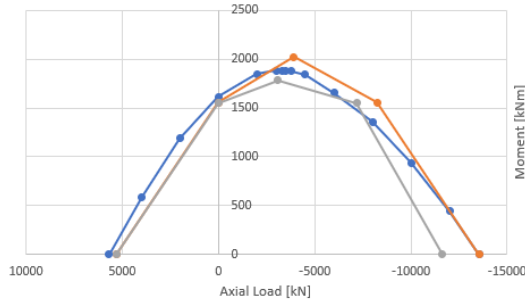


Figure 3.19: $M_z - N$ interaction domain after 30 minutes, P40x80t10

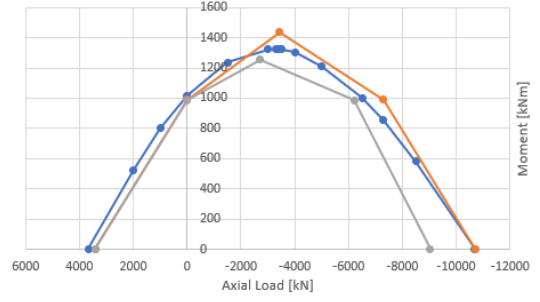


Figure 3.20: $M_z - N$ interaction domain after 60 minutes, P40x80t10

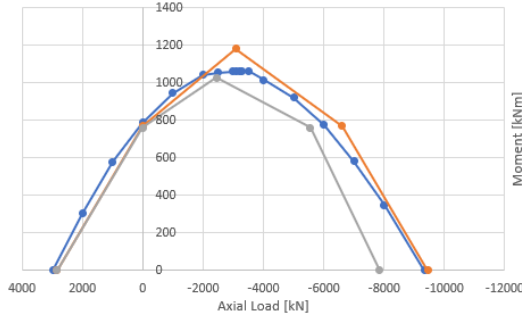


Figure 3.21: $M_z - N$ interaction domain after 90 minutes, P40x80t10

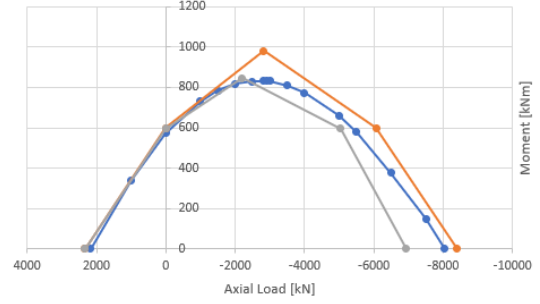


Figure 3.22: $M_z - N$ interaction domain after 120 minutes, P40x80t10

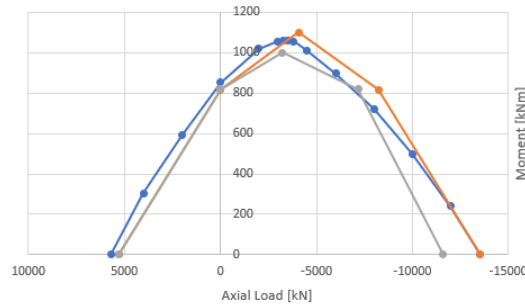


Figure 3.23: $M_y - N$ interaction domain after 30 minutes, P40x80t10

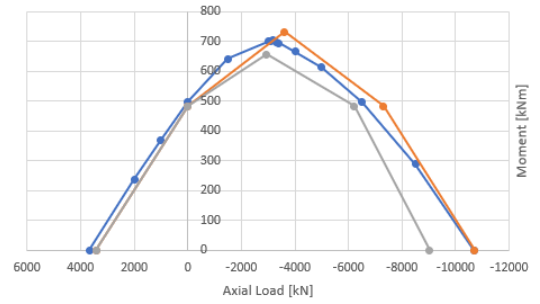


Figure 3.24: $M_y - N$ interaction domain after 60 minutes, P40x80t10

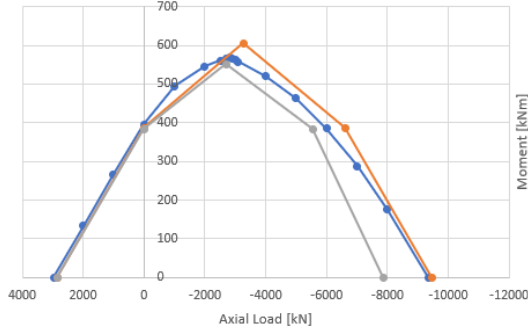


Figure 3.25: $M_y - N$ interaction domain after 90 minutes, P40x80t10

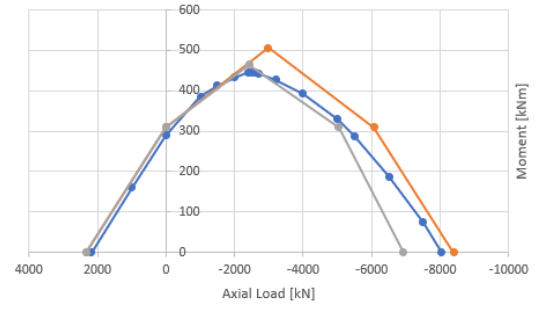


Figure 3.26: $M_y - N$ interaction domain after 120 minutes, P40x80t10

As for column P30x60t5, the same analysis was done. In this case, figures 3.27-3.30 represent the behavior in the z-axis, while figures 3.31-3.34 represent the behavior in the y-axis.

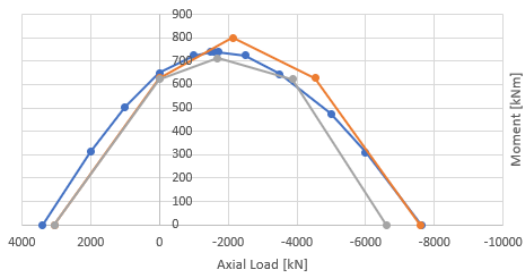


Figure 3.27: $M_z - N$ interaction domain after 30 minutes, P30x60t5

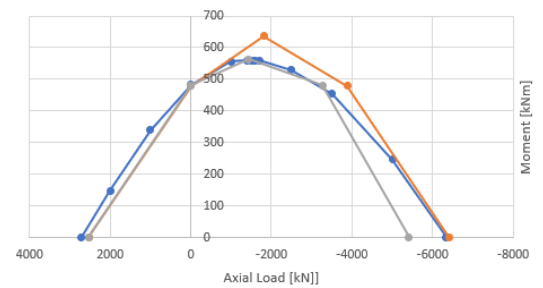


Figure 3.28: $M_z - N$ interaction domain after 60 minutes, P30x60t5

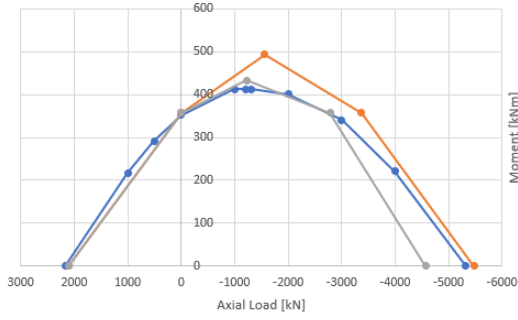


Figure 3.29: $M_z - N$ interaction domain after 90 minutes, P30x60t5

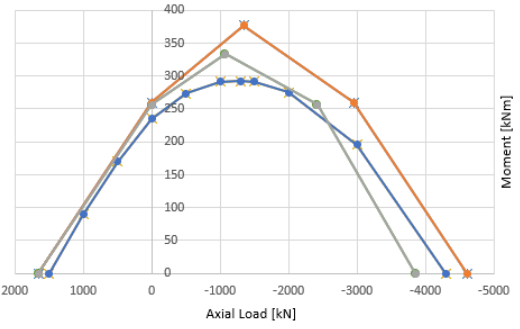


Figure 3.30: $M_z - N$ interaction domain after 120 minutes, P30x60t5

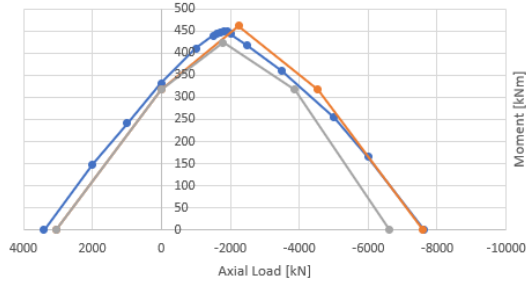


Figure 3.31: $M_y - N$ interaction domain after 30 minutes, P30x60t5

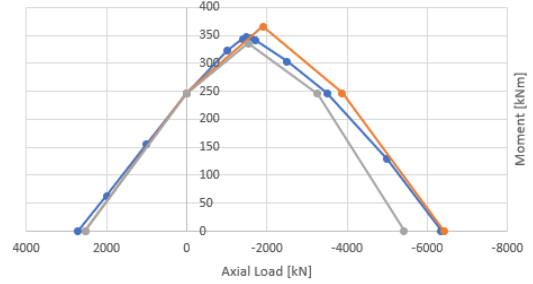


Figure 3.32: $M_y - N$ interaction domain after 60 minutes, P30x60t5

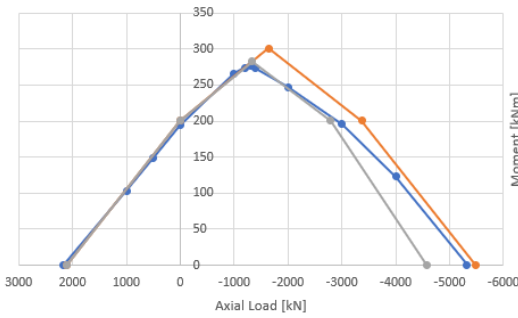


Figure 3.33: $M_y - N$ interaction domain after 90 minutes, P30x60t5

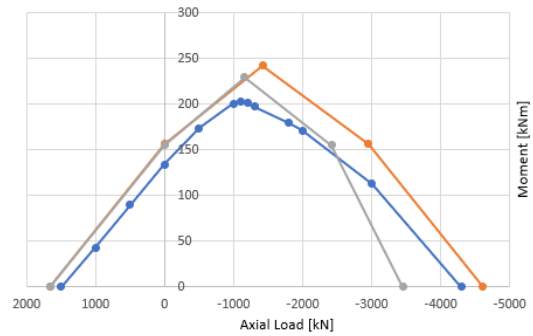


Figure 3.34: $M_y - N$ interaction domain after 120 minutes, P30x60t5

3.4 Discussion

3.4.1 Curve with SS relationship for concrete as displayed in figure 3.9

As can be observed throughout the results, this curve tends to provide generally conservative values for the compression side of the interaction domain.

It can also be noted that the peak moment value tends to be more conservative for smaller time values (e.g. for 30 minutes), while the higher time values tend to mimic more accurately the results found with the software CDM DOLMEN or even surpass them slightly. These observations can be observed quantitatively in tables 3.1 and 3.2, where the percentual difference between the results for the peak moment value obtained through the developed tool and CDM DOLMEN are evaluated.

Direction/time	Dolmen Result [kNm]	5-Point Approach Result [kNm]	Percentual Difference
Mz/120	833	845	1.44%
My/120	446.5	465	4.14%
Mz/90	1064	1027	-3.48%
My/90	567.77	552	-2.78%
Mz/60	1324.6	1256	-5.18%
My/60	703.19	657	-6.57%
Mz/30	1883	1781	-5.42%
My/30	1063.31	1000	-5.95%

Table 3.1: Accuracy of the method used, P40x80t10

Despite some overestimation of strength in some specific cases (particularly R120 for column P30x60t5), this method, when coupled with the stress-strain relationship present in Eurocode 2 part 1-2 [35], produces very similar results to those of the commercial software CDM DOLMEN, even if usually slightly on the conservative side. As such, and given that its error tends to be on the side of safety, this method can be used safely as a predesign tool for the fire resistance of reinforced concrete-filled rectangular hollow steel columns (or any kind of composite section, if necessary modifications are made).

Direction/time	Dolmen Result [kNm]	5-Point Approach Result [kNm]	Percentual Difference
Mz/120	292.3	333	13.92%
My/120	203	229	12.81%
Mz/90	413.33	433	4.76%
My/90	276.83	282.5	2.05%
Mz/60	559.98	564	0.72%
My/60	346.53	335.55	-3.17%
Mz/30	739.965	712	-3.78%
My/30	449.5	424	-5.67%

Table 3.2: Accuracy of the method used, P30x60t5

3.4.2 Curve with SS relationship for concrete as displayed in figure 3.12 (modified parabola-rectangle)

In this case, it is possible to observe that the peak moment values, and more generally all the moment couples associated with compressive axial loads, tend to be considerably higher than those produced by CDM DOLMEN. This can be observed more accurately when looking at tables 3.3 and 3.4.

Direction/time	Dolmen Result [kNm]	5-Point Approach (PR) Result [kNm]	Percentual Difference
Mz/120	833	981	17.77%
My/120	446.5	506	13.33%
Mz/90	1064	1182	11.09%
My/90	567.77	605	6.56%
Mz/60	1324.6	1439	8.64%
My/60	703.19	732	4.10%
Mz/30	1883	2024	7.49%
My/30	1063.31	1100	3.45%

Table 3.3: Accuracy of the method used, P40x80t10

Direction/time	Dolmen Result [kNm]	5-Point Approach (PR) Result [kNm]	Percentual Difference
Mz/120	292.3	377.21	29.05%
My/120	203	242	19.21%
Mz/90	413.33	494	19.52%
My/90	276.83	301	8.73%
Mz/60	559.98	637	13.75%
My/60	346.53	366	5.62%
Mz/30	739.965	801	8.25%
My/30	449.5	461	2.56%

Table 3.4: Accuracy of the method used, P30x60t5

It can be clearly seen that, given that this method coupled with this stress-strain relationship for concrete greatly overestimates the bending strength of the section, this should not be used as a predesign tool. Regardless of this, it is also possible to note that the results obtained for point 2 (fully compressed section, no moment resistance) tend to be more accurate than those obtained with the conservative stress-strain relationship for concrete.

Chapter 4

Application - Hypothesis of Recovery at Torino Esposizioni Complex

The Torino Esposizioni complex (observable in figure 4.1) was built in the 1940s, with some parts being added later in the 1960s as part of a series of renovations post-war. The complex was originally meant to be a site for the Ente Nazionale della Moda but has since seen its use vary over the years. Having been used as a site for the Salone dell'automobile di Torino and the 20th Winter Olympic Games in the past, it has largely been in disuse since then.



Figure 4.1: Torino Esposizioni Complex

The current project under study is a hypothetical recovery of part of the Torino Esposizioni complex, a 1-floor structure in disuse and a state of decay and abandonment, with problems of obsolescence and structural decay [38]. Given that

this structure is considered of low architectural significance, the current plan is to demolish the present structure and rebuild it in accordance with a new set of architectural plans which will see this building become a three-story structure that could be used for didactic purposes.

4.1 Traditional Reinforced Concrete Approach

With this objective in mind, the first possible design was made with a traditional reinforced concrete approach. This was iterative and the loads were applied through the software SAP2000, looking for a design capable of withstanding the actions associated with the ultimate limit state combinations.

As can be observed in figures 4.2-4.5, there is a need for a wide array of different columns/shear walls in order to meet all the ULS and architectural requirements. More specifically, there are 11 different sections: P60x30, P40x40, P120x30, P240x30, P80x40, P145x30, P150x30, P100x30, P130x30, P160x30 and P185x30.

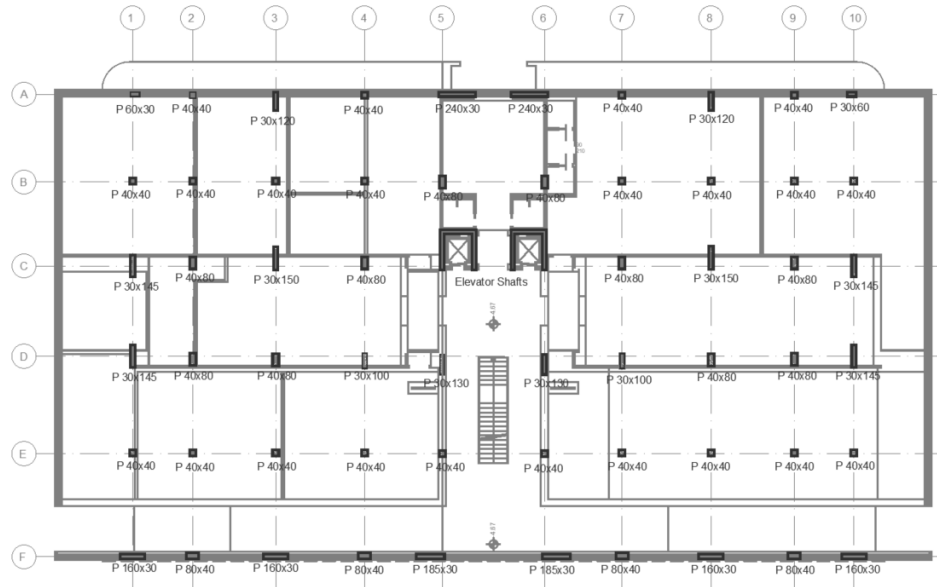


Figure 4.2: Underground floor, reinforced concrete columns

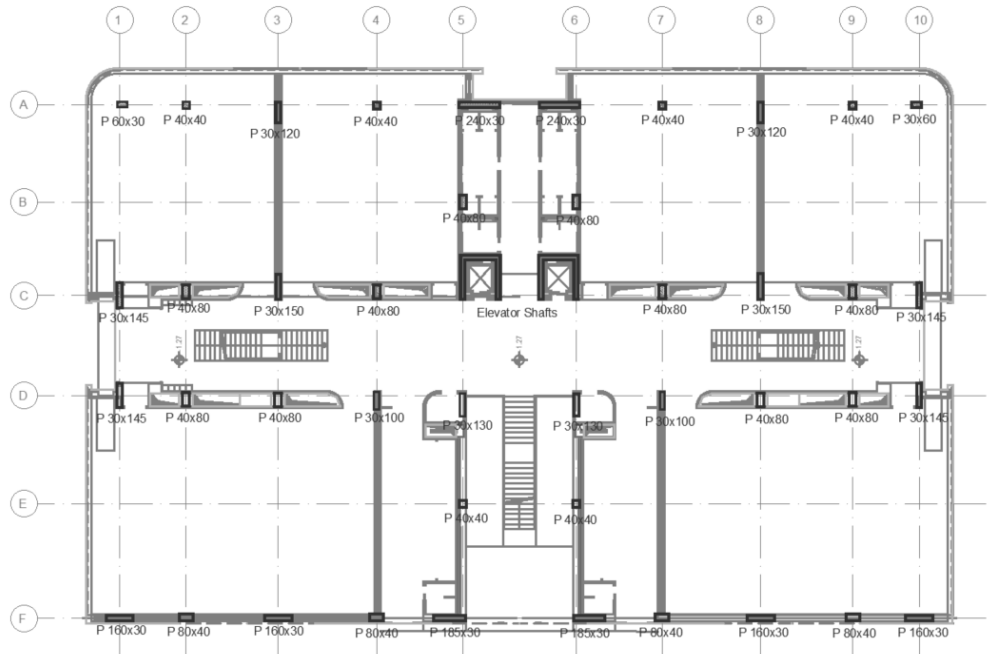


Figure 4.3: Ground floor, reinforced concrete columns

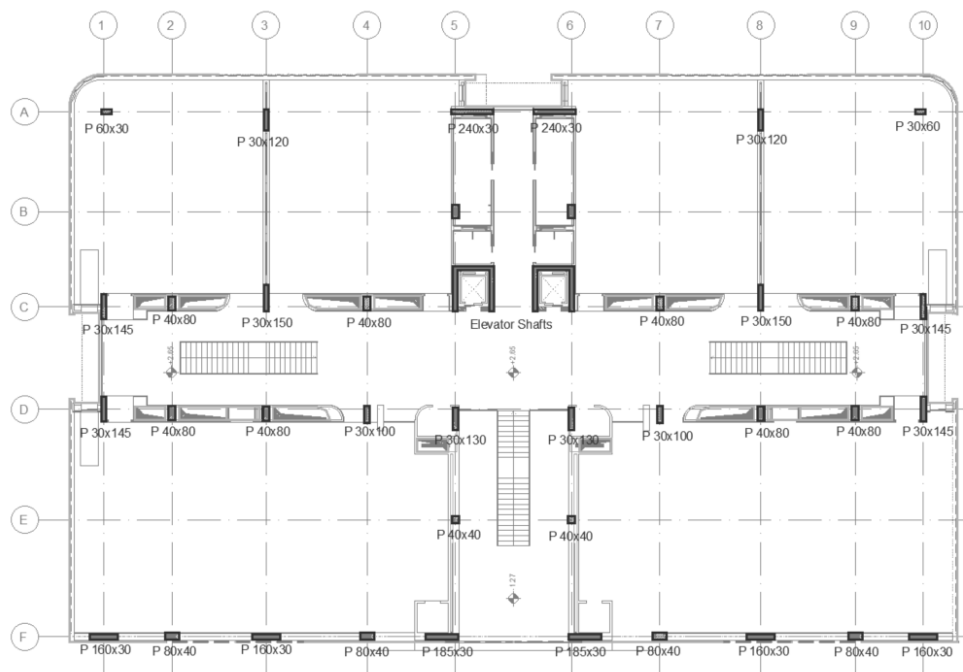


Figure 4.4: First-floor, reinforced concrete columns

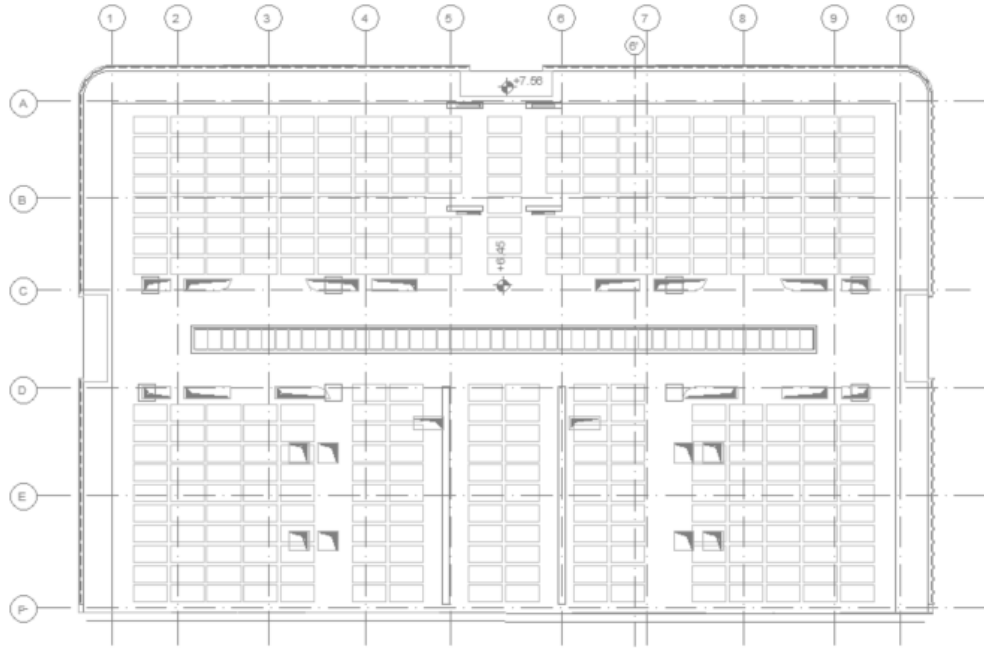


Figure 4.5: Roof structural plans

Table 4.1 shows the fire behavior of these columns, as a function of their utilization factor, their minimum dimension, and their concrete cover as per Eurocode 2, part 1-2 [35].

Column Dimensions	Fire Class
P60x30	R90
P40x40	R60
P120x30	R90
P240x30	R90
P80x40	R60
P145x30	R120
P150x30	R120
P100x30	R120
P130x30	R120
P160x30	R120
P185x30	R120

Table 4.1: Fire resistance class of RC columns in traditional approach, per the tabular method in Eurocode 2, part 1-2 [35]

It can be observed that, given the guarantee of a concrete cover of 5 cm, the

columns tend to provide relatively high fire resistance despite most of them having a relatively small minimum dimension.

4.2 Alternative Composite Column Approach

As an alternative to the previously seen approach, another design was realized with the intention of observing the advantages of a possible composite column solution, using reinforced concrete-filled rectangular hollow steel columns. The results of this design, in terms of plans, are shown in figures 4.6-4.8. The plan associated with the ceiling of the building remains the same as it is not influenced by the column design.

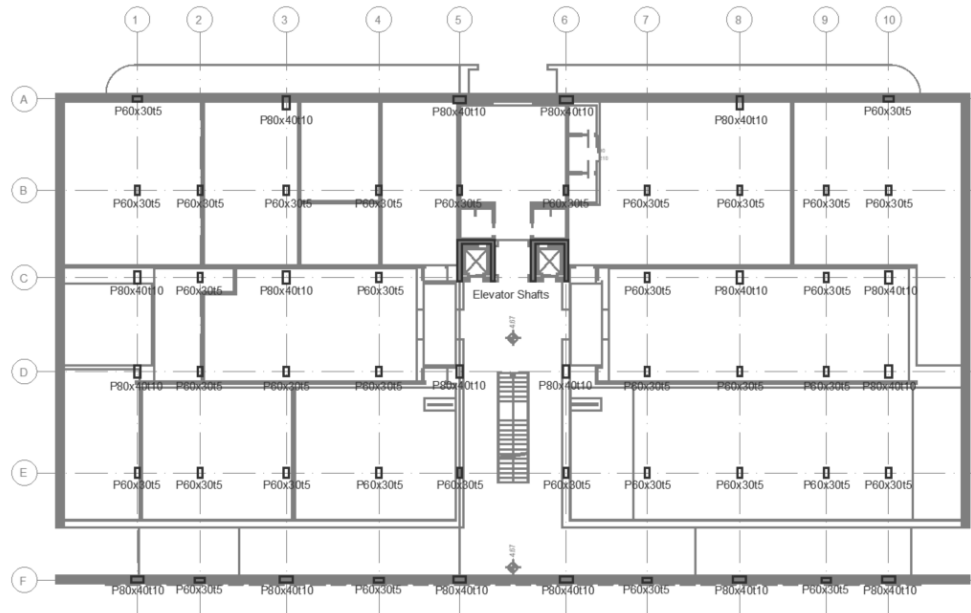


Figure 4.6: Underground floor, composite columns

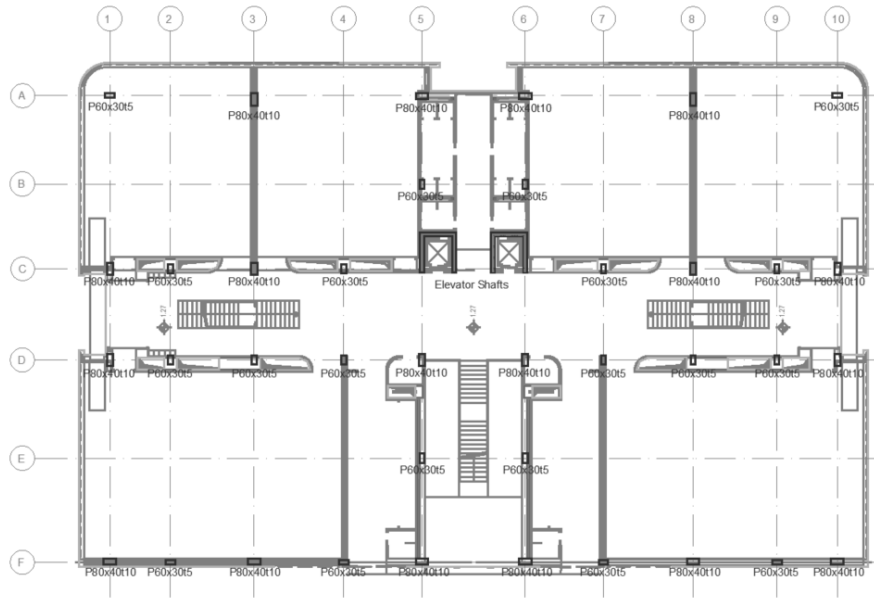


Figure 4.7: Ground floor, composite columns

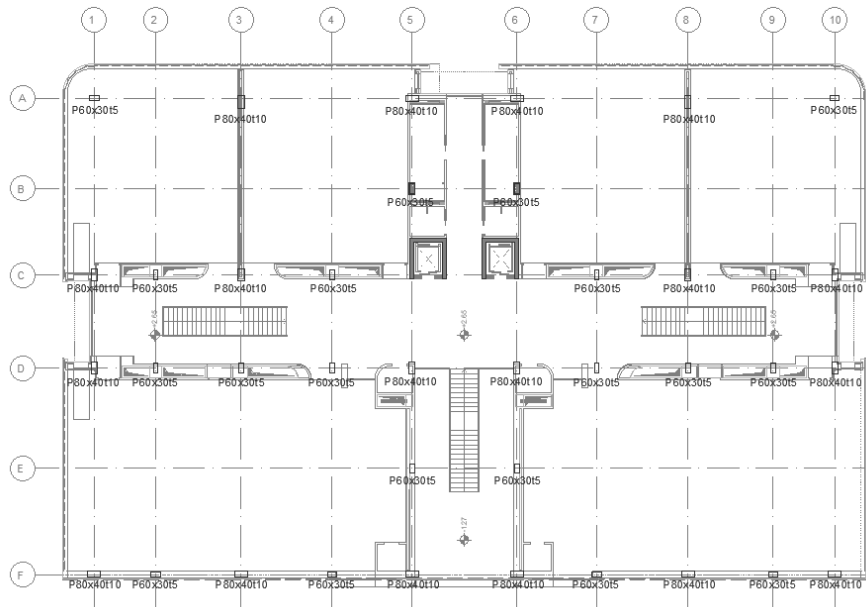


Figure 4.8: First-floor, composite columns

This was, once again, an iterative process searching for the correct column design able to withstand the ULS solicitations. The column dimensions found are those

observable in figure 4.9, where all the details are available. As for the steel profiles, these were designed using structural steel S355.

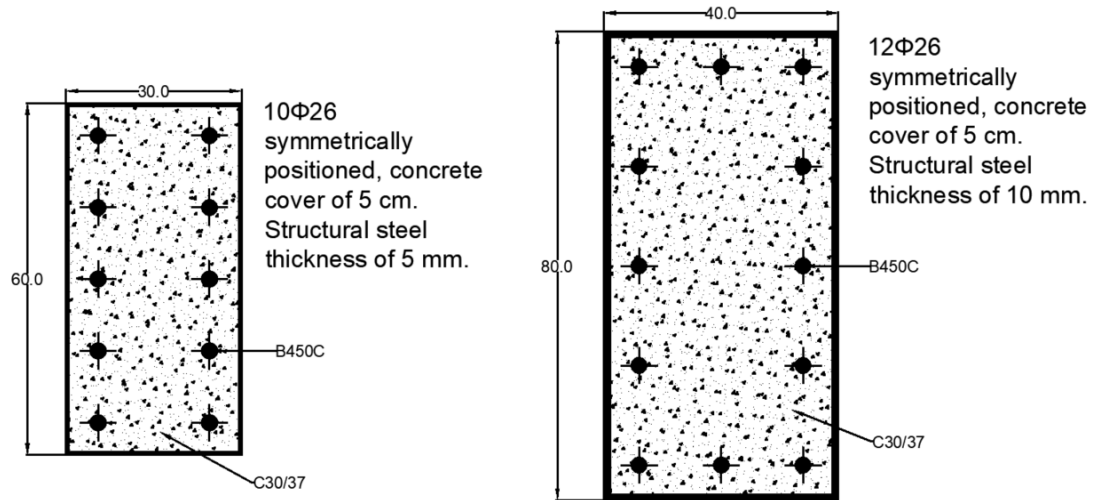


Figure 4.9: Composite columns details

The structure was then modeled on SAP2000, considering the same design for beams and slabs as present in the original reinforced concrete design, and is shown in figures 4.10 and 4.11. In the latter, green columns represent P30x60 columns, while the yellow columns represent P40x80.

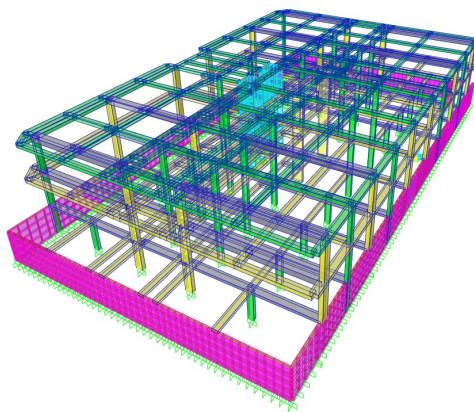


Figure 4.10: SAP2000 model

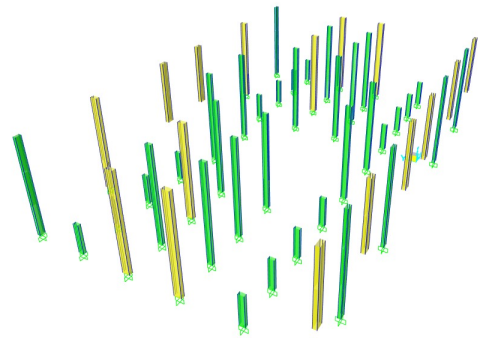


Figure 4.11: Composite columns in SAP2000 model

From these models and plans, which have been verified for the same ULS combinations as the RC approach, we can observe some clear advantages portrayed by the composite approach. Among these, some relevant advantages are:

- Design simplicity. The number of different cross-sections was reduced from 11 to 2, meaning that the analysis and design required are reduced.
- Construction simplicity. Also due to the reduction of cross sections, which constitutes a great constructional advantage in terms of organization and speed.
- Increment in usable area. The reduction in the section of the columns reduced the floor surface used by columns, increasing the usable floor surface by 11.27 m². This means that the column area decreases by more than 27%.
- No need for formwork as the steel profile is able to shape and maintain the concrete while curing.

As for the fire design, the 5-point approach detailed in the previous chapter was employed to obtain the resistance class of each column type at each level. In order to be on the safer side, the stress-strain relationship for concrete was considered with a peak value of $k \cdot f_{c,k}$ and linear descending branch until $\epsilon_{cu1,\theta}$. In this way, the interaction domain in both axes was computed for both types of columns, and the utilization factors for each direction were calculated through equations 4.1 and 4.2.

$$UF_z = \frac{M_{d,z}}{M_{Rd,z,\theta}} \quad (4.1)$$

$$UF_y = \frac{M_{d,y}}{M_{Rd,y,\theta}} \quad (4.2)$$

Aside from the uni-directional verifications, also a utilization factor considering the interaction of bending moment in both directions simultaneously was considered in accordance with Bresler's domain as shown in equation 4.3.

$$UF_{Bi} = \frac{M_{d,z}}{M_{Rd,z,\theta}} + \frac{M_{d,y}}{M_{Rd,y,\theta}} = UF_z + UF_y \quad (4.3)$$

The full detail of the classification and utilization factor in each direction for each column can be observed in figures A.1 to A.6 in Appendix A. In figures 4.12 and 4.13 it is possible to visualize a brief analysis of the most solicited P30x60 columns at each level (UG - underground, GF - ground floor, FF - first floor). The classification based on the level where a column is present is frequently utilized in

fire design. This is because the detrimental consequences of a column collapse are greater when it occurs at a lower level compared to one collapsing at higher levels.

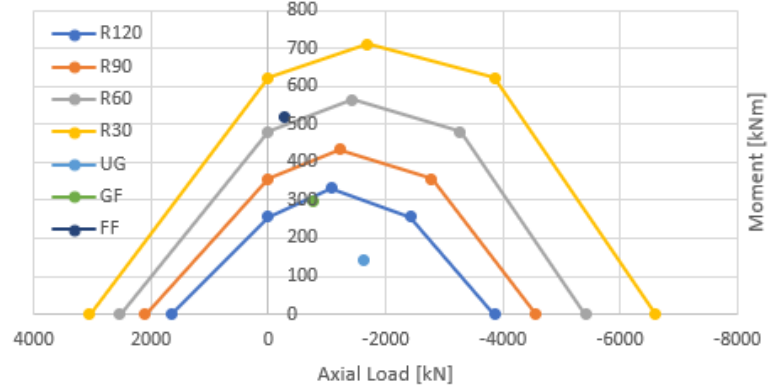


Figure 4.12: $M_z - N$ Interaction Domain, P30x60

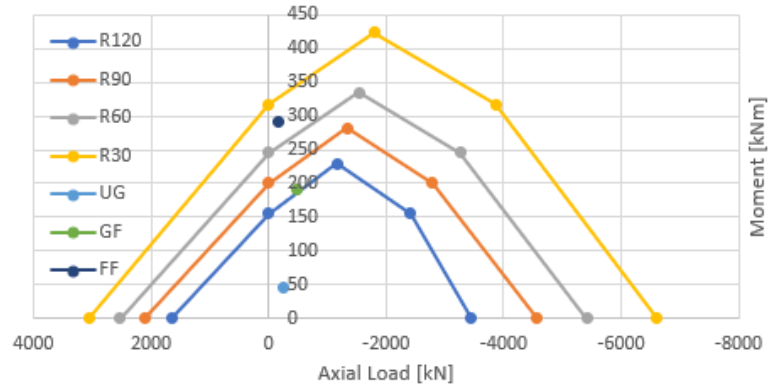


Figure 4.13: $M_y - N$ Interaction Domain, P30x60

It can be clearly observed that, as could be expected, columns on higher floors tend to achieve a lower class of fire resistance. This is due to higher moments and smaller compressive axial loads, which help bear the bending moments for the range of loading present in this structure. It is evident but regardless important to mention that the z-axis is the strong axis in these columns, while the y-axis is the one with the smaller inertia moment.

The same analysis was also done to the P40x80 columns, yielding the results observable in figures 4.14 and 4.15.

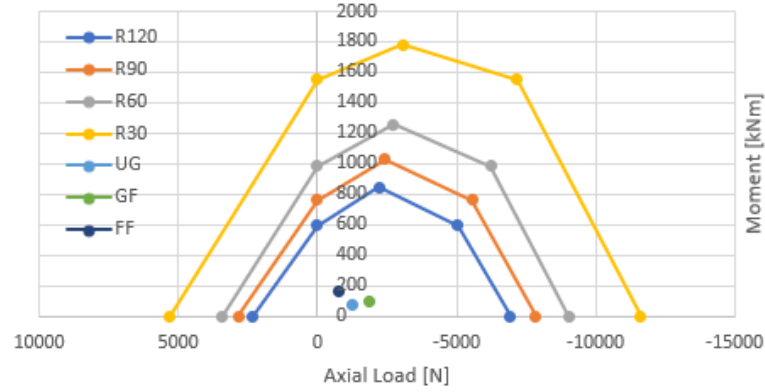


Figure 4.14: $M_z - N$ Interaction Domain, P40x80

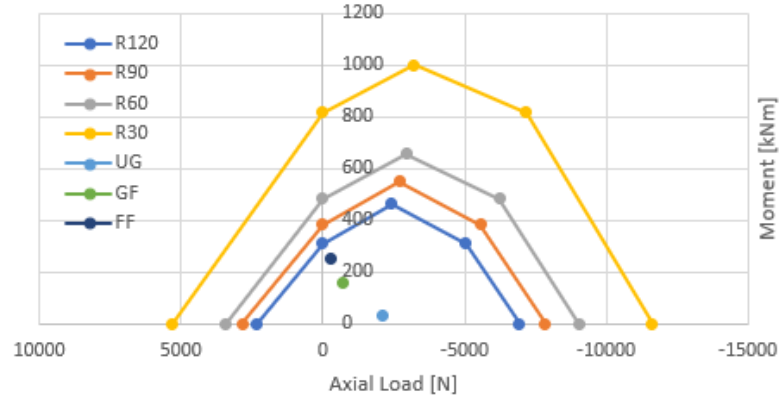


Figure 4.15: $M_y - N$ Interaction Domain, P40x80

We can observe that the same observations made for the P30x60 columns remain accurate, with the columns on higher floors being generally closer to the boundaries of the interaction domain. We can also note that the results of the P40x80 columns are safer than those seen for the P30x60 columns. This can be explained by a wide variety of motives, but chief among them are its higher nominal capacity (associated with more concrete area, thicker structural steel, and more reinforcement bars) and its elongated shape. The latter, in particular, results interesting due to its association with heat transfer within the section. The temperature of each finite element inside the section is related to its distance to sides exposed to fire, and the elongated shape allows for the concrete in the middle of the section to remain more isolated (in this case the heat only comes from two sides, as opposed to a section of more regular form where it comes from four sides).

Regardless of the result associated with each axis, we need to consider the interaction between the bending moment in both directions to establish the safety of the structure. Table 4.2 summarizes the global results obtained for the structure treated throughout this chapter.

Level	Column Type	Fire Classification	Level Classification
Under	P30x60t5	R120	R120
Ground	P40x80t10	R120	
Ground Floor	P30x60t5	R90	R90
	P40x80t10	R120	
First Floor	P30x60t5	R30	R30
	P40x80t10	R120	

Table 4.2: Fire classification of the structure

Chapter 5

Conclusions

It is possible to conclude that the 5-Point approach developed throughout this study provides sufficiently accurate and safe results to be used as a predesign tool for estimating the fire resistance of reinforced concrete-filled rectangular hollow steel columns. Additionally, its simplicity and intuitive work add value as a possible educational tool looking at a subject that is currently not easy to approach with didactic intent.

It was also noted that, given that the two stress-strain relationships considered for concrete provide higher accuracy for different points, a 5-point method considering a hybrid SS relationship for concrete might provide a tool that models better the behavior under study. This situation can be observed clearly in Figure 5.1, where this method was applied to the column with dimensions of 40x40 cm and a structural steel thickness of 10 mm, as seen in Figure 3.1.

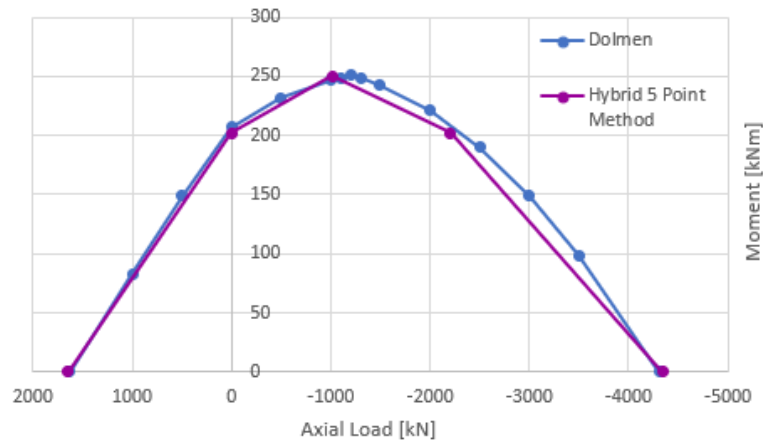


Figure 5.1: $M_z - N$ Interaction Domain, P40x40t10, Hybrid Approach

Through this hybrid approach, it is possible to model the softening behavior of the columns in an accurate and safe way (as done by the SS relationship provided by Eurocode 2, part 1-2 [35]) but still model point 5 in a way that takes full advantage of the compressive strength of concrete (as done by the modified parabola-rectangle SS relationship).

As for the use of these columns in general, it is clear that they can be competitive even in the case of fire design (which is usually one of the greatest complications when it comes to exposed steel). They can provide a wide array of advantages, ranging in kind from architectonic to structural and constructive, as have been extensively mentioned in this study, and should be seriously considered for design.

Appendix A

Detail of Utilization Factors for Composite Columns Designed

Frame ID	Mz-R120	UF_z	My-R120	UF_y	UF_Bi	CLASS
1	838.0135	0.039711	456.1555	0.005126	0.044837	R120
47	736.4635	0.08992	389.1069	0.000664	0.090584	R120
48	736.4417	0.10044	389.0945	0.00619	0.106631	R120
58	836.6175	0.006857	446.2252	0.077315	0.084172	R120
61	812.3623	0.042522	432.3924	0.061917	0.10444	R120
64	810.8659	0.011721	431.5389	0.059781	0.071502	R120
67	833.681	0.013688	444.5505	0.070538	0.084226	R120
70	838.1236	0.018089	456.0743	0.002786	0.020875	R120

Figure A.1: Under ground columns fire classification, P40x80

Frame ID	Mz-R120	UF_z	My-R120	UF_y	UF_Bi	CLASS
4	796.1072	0.043893	423.122	0.030731	0.074625	R120
59	782.1953	0.018071	415.188	0.199133	0.217204	R120
62	761.7928	0.018447	403.5524	0.144858	0.163305	R120
65	760.3843	0.008355	402.7491	0.143894	0.15225	R120
68	781.0062	0.031511	414.5098	0.202644	0.234154	R120
71	796.0933	0.038463	423.1141	0.029831	0.068294	R120
77	725.2047	0.075203	382.686	0.348642	0.423845	R120
79	725.207	0.07035	382.6873	0.347423	0.417774	R120
85	677.5219	0.023286	355.4923	0.448287	0.471574	R120
88	677.5588	0.01275	355.5133	0.449616	0.462366	R120
91	741.4516	0.004326	391.9517	0.323528	0.327853	R120
93	725.0935	0.093653	382.6226	0.35058	0.444234	R120
95	725.2082	0.089233	382.688	0.409605	0.498838	R120
97	741.4331	0.009779	391.9411	0.318091	0.32787	R120
2091	805.6794	0.116111	428.5811	0.002263	0.118374	R120
2101	805.654	0.103401	428.5666	0.005693	0.109094	R120

Figure A.2: Ground floor columns fire classification, P40x80

Frame ID	Mz-R120	UF_z	My-R120	UF_y	UF_Bi	CLASS
57	681.2395	0.245236	357.6125	0.048342	0.293578	R120
60	680.6788	0.09345	357.2927	0.484912	0.578362	R120
63	671.2617	0.12795	351.9221	0.318586	0.446535	R120
66	669.9566	0.122672	351.1778	0.332057	0.454729	R120
69	679.406	0.090276	356.5668	0.49789	0.588166	R120
72	681.2799	0.244885	357.6355	0.047724	0.292609	R120
78	649.7863	0.237863	339.6745	0.584195	0.822059	R120
80	649.7886	0.236854	339.6759	0.583999	0.820853	R120
86	628.2055	0.046847	327.3669	0.759998	0.806845	R120
89	628.2115	0.04546	327.3703	0.760201	0.805661	R120
92	656.7114	0.013293	343.624	0.128916	0.142209	R120
94	654.9714	0.223319	342.6316	0.702457	0.925776	R120
96	654.9981	0.221481	342.6469	0.699101	0.920581	R120
98	656.71	0.011375	343.6232	0.1292	0.140575	R120
2092	685.4808	0.064575	360.0313	0.029755	0.094331	R120
2102	685.4729	0.064862	360.0268	0.031896	0.096757	R120

Figure A.3: First floor columns fire classification, P40x80

Frame ID	Mz-R120	UF_z	My-R120	UF_y	UF_Bi	CLASS
2	313.296	0.295	213.403	0.148	0.443	R120
20	313.314	0.293	213.421	0.147	0.440	R120
21	267.090	0.003	164.277	0.024	0.027	R120
22	275.190	0.004	171.581	0.221	0.225	R120
23	274.819	0.059	171.246	0.268	0.327	R120
24	279.472	0.014	175.441	0.171	0.185	R120
25	308.912	0.000	201.984	0.138	0.139	R120
26	308.904	0.008	201.976	0.142	0.149	R120
51	273.360	0.090	171.911	0.011	0.101	R120
53	306.893	0.469	200.163	0.055	0.524	R120
54	273.507	0.110	172.064	0.013	0.124	R120
1592	284.135	0.007	179.645	0.003	0.010	R120
1593	282.102	0.027	177.812	0.005	0.032	R120
1594	288.656	0.007	183.721	0.010	0.017	R120
1595	288.179	0.018	183.291	0.011	0.029	R120
1596	285.850	0.029	181.191	0.001	0.029	R120
1597	288.660	0.006	183.724	0.011	0.017	R120
1598	284.151	0.004	179.659	0.003	0.007	R120
1599	282.109	0.027	177.818	0.005	0.032	R120
2027	286.574	0.028	181.843	0.007	0.035	R120
2033	282.631	0.013	178.288	0.031	0.044	R120
2035	285.849	0.029	181.191	0.002	0.030	R120
2036	288.180	0.017	183.291	0.011	0.028	R120
2037	324.203	0.204	224.735	0.030	0.234	R120
2040	331.889	0.143	224.955	0.024	0.166	R120
2049	285.653	0.009	181.014	0.021	0.030	R120
2050	327.542	0.083	228.204	0.040	0.123	R120
2053	327.166	0.102	218.441	0.026	0.128	R120
2056	298.682	0.020	198.220	0.064	0.083	R120
2062	298.672	0.017	198.210	0.067	0.085	R120
2068	327.547	0.077	228.209	0.042	0.118	R120
2071	326.957	0.105	218.253	0.032	0.137	R120
2080	285.657	0.010	181.017	0.020	0.029	R120
2081	324.418	0.183	224.958	0.034	0.216	R120
2084	331.804	0.176	225.052	0.026	0.202	R120
2112	280.558	0.460	176.420	0.011	0.471	R120
2113	282.814	0.026	178.454	0.031	0.057	R120

Figure A.4: Under ground columns fire classification, P30x60

Frame ID	Mz RX	UF_z	My RX	UF_y	UF_Bi	CLASS
5	330.382	0.401	221.340	0.095	0.496	R120
49	330.365	0.403	221.325	0.094	0.497	R120
52	302.118	0.145	201.789	0.050	0.195	R120
55	302.060	0.150	201.729	0.048	0.198	R120
2013	314.516	0.026	214.671	0.423	0.449	R120
2025	314.507	0.019	214.661	0.430	0.449	R120
2038	404.981	0.738	248.092	0.118	0.857	R90
2041	303.786	0.701	197.361	0.100	0.801	R120
2054	292.153	0.383	186.874	0.183	0.566	R120
2057	321.943	0.008	222.387	0.335	0.343	R120
2063	321.936	0.005	222.380	0.338	0.344	R120
2069	302.096	0.599	195.838	0.258	0.857	R120
2072	292.156	0.389	186.876	0.181	0.570	R120
2082	404.792	0.732	247.906	0.114	0.846	R90
2085	303.519	0.708	197.121	0.099	0.806	R120
2087	386.195	0.060	229.614	0.822	0.882	R90
2093	279.982	0.176	175.900	0.707	0.883	R120
2099	279.986	0.192	175.905	0.710	0.902	R120
2105	386.186	0.048	229.605	0.830	0.879	R90
2542	302.089	0.605	195.832	0.255	0.860	R120

Figure A.5: Ground floor columns fire classification, P30x60

Frame ID	Mz RX	UF_z	My RX	UF_y	UF_Bi	CLASS
19	287.195	0.667	182.403	0.270	0.937	R120
50	287.192	0.667	182.401	0.269	0.936	R120
56	306.941	0.470	200.206	0.053	0.524	R120
2014	303.541	0.102	197.141	0.624	0.726	R120
2026	303.559	0.102	197.157	0.626	0.728	R120
2039	638.019	0.816	334.528	0.104	0.919	R30
2042	495.941	0.714	260.995	0.106	0.820	R60
2055	269.926	0.682	166.834	0.316	0.998	R120
2058	295.682	0.056	190.055	0.593	0.649	R120
2064	295.681	0.056	190.054	0.592	0.648	R120
2070	494.740	0.602	259.790	0.305	0.907	R60
2073	269.926	0.679	166.834	0.317	0.996	R120
2083	637.835	0.814	334.321	0.108	0.922	R30
2086	494.578	0.731	259.627	0.086	0.818	R60
2088	632.776	0.034	328.641	0.891	0.925	R30
2094	488.151	0.160	253.177	0.694	0.853	R60
2100	488.154	0.161	253.179	0.694	0.855	R60
2106	632.770	0.033	328.635	0.891	0.924	R30
2541	494.741	0.601	259.791	0.304	0.905	R60
2548	398.374	0.598	189.390	0.283	0.881	R60

Figure A.6: First floor columns fire classification, P30x60

Bibliography

- [1] «EN 1990: Eurocode - Basis of structural design». In: (Dec. 2002), pp. 46–50 (cit. on pp. 1, 18).
- [2] M. I. Abdul Aleem and P. D. Arumairaj. «GEOPOLYMER CONCRETE- A REVIEW». In: (Feb. 2012), p. 1 (cit. on p. 2).
- [3] «EN 1992-1-1: Eurocode 2: Design of concrete structures - Part 1-1: General rules and rules for buildings». In: (Dec. 2004), pp. 29–40 (cit. on pp. 2, 4, 5, 8, 11, 43).
- [4] A. P. Fantilli. «Reinforced Concrete Structures Course, PoliTo». In: Materials (Oct. 2022), p. 8 (cit. on p. 3).
- [5] M. Bangash. «Concrete and concrete structures: numerical modelling and applications». In: (1989) (cit. on p. 3).
- [6] Qianmin Ma, Rongxin Guo, Zhiman Zhao, Zhiwei Lin, and Kecheng He. «Mechanical properties of concrete at high temperature — A review». In: *Construction and Building Materials* (2015), pp. 371–383 (cit. on pp. 5, 6).
- [7] Y.F. Chang, Y.H. Chen, M.S. Sheu, and G.C. Yao. «Residual stress–strain relationship for concrete after exposure to high temperatures». In: *Cement and Concrete Research* (2006), p. 2002 (cit. on p. 6).
- [8] Yu Fang Fu, Yuk Lung Wong, Chi Sun Poon, and Chun An Tang. «Literature review of study on mechanism of explosive spalling in concrete at elevated temperatures». In: *The Hong Kong Polytechnic University Department of Civil and Environmental Engineering* (2006), p. 323 (cit. on p. 7).
- [9] The Constructor, building ideas. *What is Spalling Concrete? Their causes and repair*. [Online; accessed April 29, 2023]. URL: <https://theconstructor.org/practical-guide/spalling-concrete-causes-repair/26027/> (cit. on p. 7).
- [10] L. Gardner, X. Yun, A. Fieber, and L. Macorini. «Steel Design by Advanced Analysis: Material Modeling and Strain Limits». In: (Feb. 2019), p. 2 (cit. on p. 8).

- [11] Hélder D. Craveiro, João Paulo C. Rodrigues, Aldina Santiago, and Luís Laím. «Review of the high temperature mechanical and thermal properties of the steels used in cold formed steel structures – The case of the S280 GdpZ steel». In: *Thin-Walled Structures* (2016), pp. 158–159 (cit. on p. 9).
- [12] «EN 1994-1-1: Eurocode 4: Design of composite steel and concrete structures – Part 1-1: General rules and rules for buildings». In: (Dec. 2004), pp. 64–80 (cit. on pp. 10, 12, 18).
- [13] Smeet Faldu. *Composite Columns, Madhav University*. [Online; accessed March 1, 2023]. URL: <https://madhavuniversity.edu.in/composite-columns.html> (cit. on p. 10).
- [14] Tecnostrutture. *Pilastro PDTI NPS - Vantaggi*. [Online; accessed March 2, 2023]. URL: <https://www.tecnostrutture.eu/tutti-i-prodotti-nps/strutture-verticali/pilastro-pdti-nps.html> (cit. on p. 10).
- [15] «EN 1994-1-2, Eurocode 4 - Design of Composite Steel and Concrete Structures - Part 1-2: General Rules - Structural Fire Design». In: (Aug. 2005), pp. 43–65 (cit. on pp. 14, 16, 18, 32).
- [16] «EN 1993-1-1: Eurocode 3: Design of steel structures - Part 1-1: General rules and rules for buildings». In: (May 2005), pp. 57–64 (cit. on p. 17).
- [17] T. T. Lie and R. J. Irwin. «Fire Resistance of Rectangular Steel Columns Filled with Bar-Reinforced Concrete». In: *Journal of Structural Engineering* (1995), pp. 797–805 (cit. on pp. 19–22).
- [18] «Standard Test Methods for Fire Tests of Building Construction and Materials». In: (1990), pp. 1–20 (cit. on pp. 20, 28).
- [19] T. T. Lie and V. K. R. Kodur. «Fire Resistance of Steel Columns Filled with Bar-Reinforced Concrete». In: *Journal of Structural Engineering* (1996), pp. 30–36 (cit. on p. 23).
- [20] Canadian Standard Association. «CAN/CSA-S16.1-M89: Limit States Design of Steel Structures». In: (Dec. 1989) (cit. on p. 26).
- [21] G. Grandjean, Grimault J.P, and L. Petit. «Determination de la duree au feu des profils creux remplis de beton.» In: (1981) (cit. on p. 27).
- [22] M. Chabot and T.T. Lie. «Experimental studies on the fire resistance of hollow steel columns filled with bar-reinforced concrete.» In: (1992) (cit. on p. 27).
- [23] R. S. Fike and V. K. R. Kodur. «Enhancing the Fire Performance of Concrete-Filled Steel Columns through System-Level Analysis». In: *Proceedings of the Annual Stability Conference Structural Stability Research Council* (2012) (cit. on pp. 27, 30).

- [24] «Fire-resistance tests - Elements of building construction». In: *INTERNATIONAL STANDARD ISO 834* (1975) (cit. on pp. 28, 32, 35).
- [25] S. E. Magnusson and S. Thelandersson. «Temperature-Time Curves of Complete Process of Fire Development; Theoretical Study of Wood Fuel Fires in Enclosed Spaces». In: *Civil Engineering and Building Series 65, Acta, Polytechnica, Scandinavia*. (1970) (cit. on p. 28).
- [26] João Paulo C. Rodrigues and Luís Laím. «Fire resistance of restrained composite columns made of concrete filled hollow sections». In: *Journal of Constructional Steel Research* (2017), pp. 65–76 (cit. on pp. 30–32).
- [27] Lin-Hai Han, You-Fu Yang, and Lei Xu. «An experimental study and calculation on the fire resistance of concrete-filled SHS and RHS columns». In: *Journal of Constructional Steel Research* (2003), pp. 427–452 (cit. on p. 33).
- [28] Ana Espinos, Manuel L. Romero, and Antonio Hospitaler. «Advanced model for predicting the fire response of concrete filled tubular columns». In: *Journal of Constructional Steel Research* (2010), pp. 1030–1046 (cit. on p. 33).
- [29] V. Moliner, A. Espinos, M. L. Romero, and A. Hospitaler. «Fire behavior of eccentrically loaded slender high strength concrete-filled tubular columns». In: *Journal of Constructional Steel Research* (2013), pp. 137–146 (cit. on p. 33).
- [30] M. Pagoulatou, T. Sheehan, X.H. Dai, and D. Lam. «Finite element analysis on the capacity of circular concrete-filled double-skin steel tubular (CFDST) stub columns». In: *Journal of Constructional Steel Research* (2014), pp. 102–112 (cit. on p. 33).
- [31] A. Espinos, M.L. Romero, J.M. Portolés, and A. Hospitaler. «Ambient and fire behaviour of eccentrically loaded elliptical slender concrete-filled tubular columns». In: *Journal of Constructional Steel Research* (2014), pp. 97–107 (cit. on p. 33).
- [32] TACP Oliveira. «Fire Resistance of Composite Columns Made of Concrete Filled Circular Hollow Sections and with Restrained Thermal Elongation(Ph.D. thesis)». In: *University of Coimbra, Coimbra, Portugal* (2013) (cit. on p. 33).
- [33] John H. Lienhard IV and John H. Lienhard V. *A Heat Transfer Textbook, 5th edition*. Massachusetts, U.S.A.: Phlogiston Press Cambridge, 2020 (cit. on p. 35).
- [34] Robert R. Archer, Nathan H. Cook, Stephen H. Crandall, Norman C. Dahl, Thomas J. Lardner, Frank A. McClintock, Ernest Rabinowicz, and George S. Reichenbach. *Introduction to the Mechanics of Solids*. Massachusetts, U.S.A.: Massachusetts Institute of Technology, 1978 (cit. on p. 37).

- [35] «Eurocode 2: Design of concrete structures - Part 1-2: General rules - Structural fire design». In: (July 2004), pp. 19–24 (cit. on pp. 39, 40, 44, 63, 69, 78).
- [36] «Eurocode 3: Design of steel structures - Part 1-2: General rules - Structural fire design». In: (Apr. 2005), pp. 20–23 (cit. on pp. 44, 45).
- [37] E. Cosenza, M. Di Ludovico, and C. Galasso. «Strutture in Cemento Armato. Basi della Progettazione». In: (2015), pp. 125–172 (cit. on p. 54).
- [38] «Masterplan di Ateneo - Politecnico di Torino». In: (June 2014), p. 18 (cit. on p. 66).